Forest Ecology and Management 391 (2017) 376–389

Contents lists available at ScienceDirect

Forest Ecology and Management

journal homepage: www.elsevier.com/locate/foreco

Physico-chemical and microbiological evidence of exposure effects on *Picea abies* – Coarse woody debris at different stages of decay

María Gómez-Brandón [a,*,1], Judith Ascher-Jenull [a,b,1], Tommaso Bardelli [a,b], Flavio Fornasier [c], Giulia Fravolini [d], Paola Arfaioli [b], Maria Teresa Ceccherini [b], Giacomo Pietramellara [b], Krzysztof Lamorski [e], Cezary Sławiński [e], Daniela Bertoldi [f], Markus Egli [g], Paolo Cherubini [h], Heribert Insam [a]

[a] Institute of Microbiology, University of Innsbruck, Technikerstraβe 25d, A-6020 Innsbruck, Austria
[b] Department of Agrifood and Environmental Science, University of Florence, Piazzale delle Cascine 18, 50144 Florence, Italy
[c] Consiglio per la Ricerca e la Sperimentazione in Agricoltura, Centro di Ricerca per lo Studio delle Relazioni tra Pianta e Suolo (C.R.A.-R.P.S.), Via Trieste 23, I- 34170 Gorizia, Italy
[d] Department of Bioscience and Territory, University of Molise, 86090 Pesche, Italy
[e] Institute of Agrophysics, Polish Academy of Sciences, Doświadczalna 4, 20-290 Lublin, Poland
[f] IASMA, Fondazione Edmund Mach, 38010 San Michele all'Adige, Italy
[g] Department of Geography, University of Zürich, Winterthurerstrasse 190, 8057 Zürich, Switzerland
[h] WSL Swiss Federal Institute for Forest, Snow and Landscape Research, 8903 Birmensdorf, Switzerland

ARTICLE INFO

Article history:
Received 13 December 2016
Received in revised form 13 February 2017
Accepted 14 February 2017

Keywords:
Climosequence
Wood decay
Extracellular DNA
Quantitative PCR
Hydrolytic enzymes
X-ray microtomography

ABSTRACT

Although slope aspect determines the amount of solar irradiation, with implications on the functioning of forest ecosystems, little is known yet about how this affects the aboveground deadwood decomposition dynamics. Therefore, we set up a climosequence case study to evaluate the impact of slope exposure (north- *vs.* south-facing sites) on the physico-chemical and microbiological properties of *Picea abies* coarse woody debris (CWD) at different stages of natural decay (decay classes, DCls 1–5) in an Italian Alpine setting. Variations in bacterial, fungal and archaeal abundances were assessed by real-time PCR in the extra- and intracellular DNA fractions (eDNA *vs.* iDNA) of the total deadwood DNA pool. Physico-chemical wood properties (macro- and micronutrients; lignin and cellulose content; 3D structure via X-ray microtomography) were also performed along with the determination of key enzymatic activities involved in the main nutrient cycles. Overall, higher microbial abundances were registered in *Picea abies* CWD samples at the cooler, more acidic and moister north-facing site, which are favourable conditions especially for fungal wood decomposers. This thermal signal (N > S) was more evident for the advanced decay stages (DCls 4 and 5), being wood pH the most determinant factor for discriminating between both slopes. We also found that the impact of exposure was enzyme-specific and strongly dependent on the decay class, except for those enzymes involved in the P cycle. In addition, the eDNA/iDNA ratio provided a simple yet powerful index of microbial activity in terms of exposure, with lower values at the north-facing slope indicative of a higher microbial activity. This is in line with the more pronounced physical wood damage detected at this slope by the X-ray microtomography. A higher microbial activity at the cooler north-facing site rather seems surprising – a circumstance that probably is not due to temperature itself but due to increased moisture availability at this slope.

1. Introduction

Deadwood is an important structural and functional component of forest ecosystems, acting as a temporal store of plant nutrients and water, and providing shelter and nutrition to various organisms, primarily fungi and saproxylic insects (Floudas et al., 2012; Harmon et al., 1986; Zuo et al., 2016). Moreover, deadwood represents a global carbon store estimated to be in the range of 73 ± 6 Pg (Pan et al., 2011), making its decomposition dynamics a determinant of the soil carbon balance and forest productivity (Bradford et al., 2014). However, as pointed out by Lombardi et al. (2013), in European cool to temperate and Mediterranean forest ecosystems deadwood is still poorly described and there is a paucity of information on its contribution to soil carbon and nutrient pools and to long-term forest sustainability.

* Corresponding author.
E-mail address: maria.gomez-brandon@uibk.ac.at (M. Gómez-Brandón).
[1] Both authors contributed equally to this paper.

http://dx.doi.org/10.1016/j.foreco.2017.02.033
0378-1127/

Microorganisms, particularly fungi, are key determinants of lignocellulose decomposition thanks to the secretion of a battery of oxidoreductases and hydrolases (Purahong et al., 2016) and, therefore, of deadwood decomposition in forest ecosystems (Fischer et al., 2012). Through their presence as spores in the atmosphere or even as mycelial filaments in the surrounding soil, fungi are always in the vicinity of living, dying and dead wood (Hoppe et al., 2015a). It has also been shown that wood-inhabiting fungi may benefit from wood-colonising bacteria if they metabolise toxic intermediates and/or provide fungi with limiting nutrients like iron or nitrogen via nitrogen-fixation (de Boer and Van der Wal, 2008; Hoppe et al., 2014; Valášková et al., 2009). It is known that N availability in deadwood is highly restricted, with a C to N ratio ranging from 350 to 800, which suggests that wood-inhabiting fungi may benefit from associations with N-fixing bacteria to fulfil their N requirements for vegetative and generative growth (Hoppe et al., 2014). On the other hand, wood-inhabiting bacteria may potentially confer negative effects to fungi, as they compete for easily degradable substrates that are necessary for fungal colonization and degradation activities (Folman et al., 2008). Although the direct contribution of bacteria to wood decomposition rate and dynamics seems to be smaller than that exerted by fungi, bacterial communities might play a more important role in deadwood turnover than previously thought and ultimately, in nutrient cycling in forest ecosystems (Hervé et al., 2016; Hoppe et al., 2014, 2015b; Johnston et al., 2016).

The so-called five-decay class system has commonly been used to describe the wood decay progression in the field (Harmon et al., 2013; Hunter, 1990; Lombardi et al., 2013; Petrillo et al., 2015, 2016). As woody material decays, its physical and chemical quality gradually changes and consequently a microbial community succession takes place as species are replaced by those more suited to the substrate (Rajala et al., 2012). In this regard, a climosequence approach may provide insight into deadwood decay dynamics in response to thermal conditions represented by different altitudes and exposure (Fravolini et al., 2016; Petrillo et al., 2015, 2016).

The aim of the present study was to evaluate the shifts in the wood-inhabiting microbiota of *Picea abies* (L.) Karst at different stages of decay at two subalpine sites located at north and south exposure in the Italian Alps (Val di Rabbi, Trentino) to account for different thermal conditions. Variations in bacterial, fungal and archaeal abundances with exposure were assessed in the extra- and intracellular DNA fractions (eDNA *vs.* iDNA) of the total deadwood DNA pool and related to specific physico-chemical properties of wood (i.e., pH, macro-micronutrients; lignin and cellulose content); as well as to the potential activities of key enzymes involved in the main nutrient cycles. In addition, we were interested in better characterising the structural organisation of the deadwood because it may distinctly affect the decay processes (Mayo et al., 2010; Sedighi Gilani et al., 2014).

We hypothesised that: (1) warmer climatic conditions at south exposure will favour the deadwood decomposition in terms of microbial biomass and activity; (2) the exposure-effects on deadwood physico-chemical and microbiological properties will be more evident for the advanced decay stages; (3) the eDNA/iDNA ratio will provide a simple yet powerful index of microbial activity (the lower the ratio, the higher the activity) as a function of exposure and progressing wood decay.

2. Material and methods

2.1. Study sites and sampling strategy

The investigation area was located in Val di Rabbi (Trentino) in the south Alpine belt in northern Italy. The two study sites were located at an altitude of 1930 and 1995 m a.s.l. at north (N) and south (S)-facing slopes, respectively (Egli et al., 2006). The main characteristics of the N-facing slope were: aspect 20°N; slope 12°; mean annual air temperature (MAAT) 1.4 °C; mean annual precipitation (MAP) 1180 mm yr^{-1}; while the S-facing slope was characterised by: aspect 160°N; slope 25°; MAAT 4.4 °C; MAP 1180 mm yr^{-1} (Petrillo et al., 2015). Both study sites were on acidic paragneiss or morainic parent material consisting of paragneiss (Egli et al., 2006; Petrillo et al., 2015).

Coarse woody debris (CWD) samples from decaying Norway spruce (*Picea abies* (L.) Karst) were collected in August 2013 as described by Petrillo et al. (2015). Norway spruce constitutes the dominant tree species in these study sites together with the co-occurring European larch (*Larix decidua* Mill.) (Petrillo et al., 2015, 2016). CWD samples were classified *in-situ* using the five decay class system based on visual, geometric and tactile features according to Hunter (1990): (1) hard wood, penetrable with a knife to only a few mm, bark and twigs (diameter < 1 cm) intact; (2) rather hard wood, penetrable with a knife to less than 1 cm, bark and twigs begin to shed away, branches (diameter 1–4 cm) intact; (3) distinctly softened wood, penetrable with a knife to approximately 1–4 cm, bark and branches partially lost, original log circumference intact; (4) considerably decayed wood, penetrable with a knife to approximately 5–10 cm, bark lost in most places, original log circumference begins to disintegrate; (5) wood that disintegrates either to a very soft crumbly texture or is flaky and fragile, penetrable with a knife to more than 10 cm, original log circumference barely recognizable or not discernable.

Briefly, at each site five replicates for each decay class were collected, resulting in a total of 50 samples (2 study sites × 5 decay classes × 5 field replicates). Each field replicate was a composite sample deriving from 5 sub-samples that were pooled together in the field. The CWD volume assessment of each decay class was assessed as shown by Petrillo et al. (2015). All CWD samples were placed in a coolbox until they were taken to the laboratory, where before analyses they were pulverized using a cutting-mill (Fritsch-Pulverisette; 4 mm). After each sample, drill bits were cleaned by air-brushing and rinsed with distilled water between samples. All drill dust samples from each decay class were placed in a single sterilised vinyl bag and stored at 4 °C and −20 °C for physico-chemical and (micro)biological characterisation, respectively. For X-ray microtomography analyses, untreated (not cut-milled) wood samples were stored at −20 °C (as described in Section 2.7).

2.2. Physico-chemical analyses

Cut-milled CWD samples (5 g, fresh weight) were placed into a Petri dish and oven-dried (105 °C) for at least 24 h in order to determine the dry mass of the different decay classes. The volatile solids (VS) content was determined from the mass loss following ignition in a muffle furnace (Carbolite, CWF 1000) at 550 °C for 5 h. Electrical conductivity (EC) and pH were determined in wood:water extracts (1:5, w/v) by using a conductivity Meter LF 330 WTW (Weilheim, Germany) and a pH Meter Metrohm 744, respectively. Ammonium content was measured in 0.0125 M $CaCl_2$ extracts as described by Kandeler (1993). Total C and N were determined using a CN analyser (Vario Macro CN, Elementar, Hanau, Germany– combustion analysis). The concentration of P, K, Ca, Mg, Fe and Mn was assessed by using ICP-OES (Optima 8300, Perkin Elmer, Waltham, USA) after acid digestion of 0.5 g of powdered wood with 4 mL of HNO_3 in a closed vessel (UltraWAVE Milestone, Shelton, CT, USA – maximum temperature 230 °C). The α-cellulose content was assessed following the protocol of Leavitt and Danzer (1993) and Boettger et al. (2007). The Klason lignin, which is insoluble in strong acid, was determined according to Dence and Lin

(1992) in a sequential extraction where first the water-soluble compounds were extracted. Ultrapure water (80 °C) was then added to each sample (1 g fw) and stirred 3 times for 15 min. Afterwards, the samples were centrifuged, dried and washed with ethanol as described by Fravolini et al. (2016). The supernatants were then discarded before adding ethanol again and filtering the samples. The filters were dried overnight at 60 °C followed by the addition of 3 mL of sulphuric acid (72%) to 300 mg of the filter cake. After autoclaving for 1 h at 120 °C, the resulting solution was filtered into ceramic crucibles and the liquid evaporated at 110 °C, before weighing the lignin in the crucibles (Klason lignin). The acid-soluble lignin (ASL; Klason, 1893) in the filtrate was measured photometrically at 250 nm (Cary 50 conc UV–Visible Spectrophotometer). The total lignin is the sum of the ASL + the Klason lignin; this lignin fraction also includes other recalcitrant compounds, such as tannins, cutin and suberin.

2.3. Sequential extraction of extra- and intracellular DNA

The sequential DNA extraction approach proposed by Ascher et al. (2009) for the soil metagenome was adopted to discriminate the extracellular (eDNA) and the intracellular (iDNA) fraction of the total deadwood DNA pool. Two technical replicates were included per each sample. Briefly, eDNA was extracted by gentle washings of 0.1 g cut-milled wood (fw) with 500 µL of 0.12 M Na_2HPO_4 at pH 8 in microcentrifuge tubes (2 mL) and horizontally shaken for 30 min (100 movements/min). The slurry was then centrifuged (4 °C, 30 min at 7500 g) and the supernatant collected. The wood pellet was subjected to the same procedure for two more cycles; the supernatants were pooled resulting in a final volume of 1.5 mL containing crude eDNA. Intracellular DNA was extracted from the residual pellet after the extraction of eDNA. The pellet was resuspended in 978 µL of 0.12 M Na_2HPO_4 at pH 8 and 122 µL MT buffer, transferred to tubes containing a lysing matrix (Lysing Matrix E; Fast DNA Kit for Soil; MP-Biomedicals) and one 1/4″ Ceramic sphere (MPI biochemical cat. # 6540-424) to guarantee a complete disruption of the wood tissue. The samples were then processed by a combined mechanical-chemical cell lysis using the FastPrep instrument in combination with the reagents included in the Fast DNA Kit for soil. Bead beating conditions were 40 s at a speed equal to 5.5 m/min. The DNA extracts (eDNA; iDNA) were purified using the GeneClean procedure (MP-Biomedical) in order to reach PCR compatibility. DNA extracts were quantitatively and qualitatively characterised by PicoGreen based fluorimetry (*ds*DNA; Qubit, LifeTechnologies), µL-spectrophotometry (PicoDrop) and agarose-gel electrophoresis (Ascher et al., 2012). DNA yields (eDNA *vs.* iDNA) were expressed as µg DNA g^{-1} wood (dry weight). Furthermore, the eDNA/iDNA ratio – as a function of proceeding decay status and exposure – was calculated as an estimator of microbial activity.

2.4. Quantitative real-time PCR (qPCR)

Real-time PCR was performed to quantify the microbial groups shown in Table 1 from both the eDNA and iDNA fractions of the total deadwood DNA pool with the 1X Sensimix™ SYBR® Hi-rox (Bioline, USA) based on the DNA-intercalating dye SYBR Green I. The Rotorgene 6000 Real Time Thermal Cycler (Corbett Research, Sydney, Australia) was used in combination with the Rotor-Gene Series Software 1.7. To build the standards we used purified PCR products of known concentrations from the pure cultures shown in Table 1. Stock concentration [gene copies μL^{-1}] was determined via PicoGreen measurement and freshly prepared. Ten-fold dilutions ranging from 10^8 to 10^2 copies μL^{-1} were applied for the standard curve construction. Quantitative PCR was performed in 20-µL assays with each reaction mix containing 1X Sensimix™

Table 1
Thermal profiles and primer pairs used for real-time PCR quantification of the different microbial groups assessed in the five deadwood decay classes.

Target group	Source of standard	Thermal profile	Primer	Annealing position	Amplicon length (bp)	References
Bacteria	*Nitrosomonas europaea* DSMZ 21879	95 °C–20 s/58 °C–15 s/72 °C–30 s	1055f, 1392r	16rDNA	352	Ferris et al. (1996)
Ammonia-oxidising bacteria (AOB)	*N. europaea* DSMZ 21879	95 °C–20 s/64 °C–15 s/72 °C–15 s	CTO189fA/B, CTO 189fC, RT1r	16rDNA	116	Kowalchuk et al. (1997), Hermansson and Lindgren (2001)
Nitrobacter sp.	*Nitrobacter winogradsky* DSMZ 10237	94 °C–20 s/58 °C–15 s/72 °C–20 s	1198f, 1423r	16rDNA	227	Graham et al. (2007)
Ammonia-oxidising bacteria (AOB)	Plasmid containing an *amoA* sequence	95 °C–25 s/57 °C–25 s/72 °C–40 s	amoA1F, amoA2R	*amoA* gene	491	Rotthauwe et al. (1997)
Ammonia-oxidising archaea (AOA)	Plasmid containing an *amoA* sequence	95 °C–25 s/53 °C–25 s/72 °C–40 s	Arch-amoAF, Arch-amoAR	*amoA* gene	635	Francis et al. (2005)
Nitrogen-fixing bacteria	*Azospirillum irakense*	95 °C–45 s/55 °C–45 s/72 °C–45 s	nifHf, nifHR	*nifH* gene	432	Rosch et al. (2002), Töwe et al. (2010)
Archaea	*M. formicicum* DSMZ1535	94 °C–30 s/57 °C–40 s/72 °C–30 s	Parch519f, Arc915r	16rDNA	420	Øvreås et al. (1997), Coolen et al. (2004)
Genus *Methanosaeta*	*M. concilii* DSMZ 2139	95 °C–20 s/60 °C–20 s/72 °C–20 s	MS1b, SAE835r	16rDNA	266	Shigematsu et al. (2003), Goberna et al. (2010)
Genus *Methanosarcina*	*M. barkeri* DSMZ 800	95 °C–20 s/64 °C–20 s/72 °C–20 s	240f, 589r	16rDNA	366	Franke-Whittle et al. (2009)
Genus *Methanobacterium*	*M. formicicum* DSMZ 1535	95 °C–20 s/58 °C–20 s/72 °C–20 s	fMbium, 748r	16rDNA	191	Goberna et al. (2010)
Genus *Methanosphaera*	*M. stadtmanae* DSMZ 3091	95 °C–20 s/61 °C–20 s/72 °C–20 s	594f, 747r	16rDNA	170	Goberna et al. (2010)
Genus *Methanoculleus*	*M. thermophilus* DSMZ 2640	95 °C–20 s/65 °C–20 s/72 °C–20 s	298f, 586r	16rDNA	308	Franke-Whittle et al. (2009)
Fungi	*Fusarium solani*	95 °C–15 s/50 °C–30 s/72 °C–30 s	FF390, FR1	18rDNA	390	Vainio and Hantula (2000), Prévost-Bouré et al. (2011)

In all real-time PCR runs an initial denaturing step of 10 min at 95 °C was applied. Cycle repetitions were 40 for all the runs.
f = forward, r = reverse.
Primer CTO189f A/B and primer CTO189C were used in a ratio 2:1.

Table 2
Overview of the potential enzymatic activities and their corresponding buffers and substrates evaluated in the present study.

Abbreviation	Enzyme	Buffer	Substrate	Biogeochemical cycle
aryS	Arylsulphatase	MES 200 mM pH 6	4-methylumbelliferyl sulfate	S
chit	Chitinase	MES 200 mM pH 6	4-methylumbelliferyl-N-acetyl-beta-D-glucosaminide	N
leu	Leucine-aminopeptidase	THAM 200 mM pH 7.5	L-Leucine 7-amido-4methyl-coumarine hydrochloride	N
trip	Tripsin- and papain-like protease	THAM 200 mM pH 7.5	N-alpha-CBZ-L-Arginine 7-amido-4-methylcoumarin hydrochloride	N
alfaG	Alfa-glucosidase	MES 200 mM pH 6	4-methylumbelliferyl-alpha-D-glucopyranoside	C
betaG	Beta-glucosidase	MES 200 mM pH 6	4-methylumbelliferyl-beta-D-glucopyranoside	C
cell	Cellulase	MES 200 mM pH 6	4-methylumbelliferyl-beta-D-cellobioside	C
xil	Xilosidase	MES 200 mM pH 6	4-methylumbelliferyl-beta-D-xilopyranoside	C
uroni	Glucuronidase	MES 200 mM pH 6	4-methylumbelliferyl-beta-D-glucuronide	C
ester_ac	Acetate-esterase	MES 200 mM pH 6	4-methylumbelliferyl acetate	C
ester_nona	Nonanoate-esterase	THAM 200 mM pH 7.5	4-methylumbelliferyl nonanoate	C
ester_palm	Palmitate-esterase	THAM 200 mM pH 7.5	4-methylumbelliferyl palmitate	C
acP	Acid phosphomonoesterase	MES 200 mM pH 6	4-methylumbelliferyl phosphate	P
alkP	Alkaline phosphomonoesterase	THAM 200 mM pH 9	4-methylumbelliferyl phosphate	P
bisP	Phosphodiesterase	THAM 200 mM pH 7.5	bis(4-methylumbelliferyl) phosphoric acid	P
piroP	Pyrophosphate-phosphodiesterase	THAM 200 mM pH 7.5	bis(4-methylumbelliferyl) pyrophosphoric acid	P
inosit	Inositol-phosphatase	MES 200 mM pH 6	4-methylumbelliferyl myo-inositol-1-phosphate	P

SYBR® Hi-rox, forward and reverse primers (200 nM each primer), 0.4 mg mL^{-1} BSA, distilled water (RNase/DNase free, Gibco™, UK) and 2 μL of either 1:10 diluted DNA-extract (for bacteria, archaea, fungi, AOB16S, *Nitrobacter* sp.); or undiluted DNA (for the 5 genera of methanogens, and N-cycle related functional genes); and ten-fold diluted standard DNA. For the primers used see Table 1. All standards and samples were run in duplicate following the cycling conditions in Table 1. To check for product specificity and potential primer dimer formation, runs were completed with a melting analysis starting from 60 °C to 95 °C with temperature increments of 0.25 °C and a transition rate of 5 s. The purity of the amplified products was also checked by the presence of a single band of the expected length on a 1% agarose gel stained with the DNA stain Midori Green (Nippon Genetics, Germany).

2.5. Double-stranded DNA content quantitation as estimator of microbial biomass

Determination of *ds*DNA content was carried out according to Fornasier et al. (2014) with the following modifications: an amount of 60–180 mg of cut-milled wood was weighed in duplicate in 2-mL Eppendorf tubes, by adding 1.20 mL of 0.12 M, pH 7.8, Na-phosphate buffer (Ascher et al., 2009), together with two 1/4″ ceramic spheres (MPI biochemical cat. # 6540-424). Tubes were then subjected to bead-beating using a Retsch MM400 beating mill set at 30 Hz for 120 s, followed by centrifugation at 20,000*g*. Twenty μL of supernatant containing crude total DNA were taken and diluted in TE (TRIS 10 mM; EDTA 1 mM; pH 7.5) buffer as necessary (111–221 times). Afterwards, 25 μL of diluted extract were pipetted in duplicate into 384-well black microplates for determination of *ds*DNA content using Pico-Green reagent (Life Technologies) and a fluorimeter (Synergy HT microplate reader; BIO-TEK).

2.6. Potential enzymatic activities

Seventeen hydrolytic enzymatic activities involved in C, N, P and S biogeochemical cycles (Table 2) were measured in wood extracts by applying a heteromolecular exchange process (Fornasier and Margon, 2007). The procedure was similar to that used for *ds*DNA extraction-quantification with the following modifications: extraction buffer consisted in a 3% lysozyme solution in 0.1 M NaCl, pH 6.7; and the bead-beating lasted 180 s. After centrifugation, 750 μL of supernatant were taken and diluted with 250 μL of TRIS 50 mM, pH 7.0 buffer. Twenty μL of diluted extracts were pipetted in duplicate on 384-well microplates with 40 μL of appropriate buffer in order to determine fluorometrically the different potential enzyme activities by using the substrates listed in Table 2. Each microplate was read 4 times at time intervals of 5–180 min, according to the intensity of each enzyme using a Synergy HT microplate reader (BIO-TEK). All the measurements were performed in duplicate for each field replicate and the activities were expressed as nanomoles of 4-methyl-umbelliferyl (MUF) min^{-1} g^{-1} dry wood.

2.7. X-ray microtomography analyses

CWD samples were firstly dried 24 h at 50 °C and then cut into dimensions of 3 × 3 × 10 mm in order to achieve the best contrast for computational X-ray microtomography (μCT) analyses, which were carried out using the GE Nanotom S device at the IA PAS microtomography facility. During the μCT scanning the sample was rotated to register 2D-images of the scanned samples. Based on these 2D-images a 3D-sample structure was recovered using reconstruction software. In order to reduce the potential noise, a 2D-image was acquired for each angular position of the different samples, resulting in an average value of 25 images recorded with slight (few pixels), random, perpendicular to X-ray beam detector movements. The resolution of the registered 2D images was 2284 × 2304 pixels and they were 14-bit depth grey level. The spatial resolution of 3D reconstructed volume – voxel size – was 1 μm. The X-ray source parameters were the following: accelerating voltage of 45 kV, cathode current of 350 μA and tungsten exit window.

Although the temperature in μCT chamber remains stable during the scan, the sample itself is heated by X-rays, which can cause slight thermal sample dimension changes. This could interfere for the 1-μm resolution scans during the reconstruction phase. To avoid this, a 0.5 h pre-scan was conducted prior to the main scan. For the 3D volume reconstruction the DatosX 2.0 software was chosen, which resulted in 2284 × 2284 × 2304 16 bit grey level volume. For image analysis, processing and visualization VG Studio 2.0, Avizo 9 and Fiji software were used. The basic procedure for image processing involved the selection of the region of interest (ROI), along with the application of 3D median filtering with the kernel diameter equal to 3 px. The following nomenclature for ortho-views was used in this study: *tangential view*/*cross section* –cross section by the plane normal to tangential direction; *radial view*/*cross section* –cross section by the plane normal to radial direction; and *longitudinal view*/*cross section* –cross section by the plane normal to longitudinal direction.

Table 3
Physico-chemical properties and elemental concentrations in the decay classes 1–5 from the north- and south-facing slopes. Values are means ± standard deviation. Data are given on a dry weight basis.

	North-facing slope					South-facing slope				
Decay classes	1	2	3	4	5	1	2	3	4	5
Moisture (%)	26 ± 6	31 ± 7	47 ± 17	69 ± 5	64 ± 8	14 ± 1	14 ± 3	18 ± 6	44 ± 18	74 ± 1
VS (%)	99 ± 0.6	99 ± 0.3	100 ± 0.3	99 ± 0.7	68 ± 11	99 ± 0.4	99 ± 0.4	100 ± 0.1	100 ± 0.3	99 ± 0.5
pH	4.1 ± 0.1	4.0 ± 0.1	3.8 ± 0.2	3.9 ± 0.1	4.2 ± 0.1	5.0 ± 0.2	4.3 ± 0.5	4.8 ± 0.5	4.7 ± 0.1	4.6 ± 0.3
EC ($\mu S\ cm^{-1}$)	145 ± 4	160 ± 26	67 ± 14	66 ± 16	63 ± 14	173 ± 11	160 ± 28	111 ± 14	86 ± 12	45 ± 1.5
Total N ($g\ kg^{-1}$)	2.2 ± 0.5	1.3 ± 0.1	1.0 ± 0.1	4.3 ± 0.3	6.2 ± 1.0	1.8 ± 0.6	1.2 ± 0.2	1.3 ± 0.2	2.3 ± 0.2	3.3 ± 0.4
NH_4^+ ($mg\ kg^{-1}$)	6.5 ± 0.5	1.4 ± 0.08	1.5 ± 0.1	2.5 ± 0.5	13.8 ± 4.2	6.3 ± 2.5	4.2 ± 0.6	6.3 ± 2.8	6.1 ± 1.8	6.2 ± 2.7
Total C (%)	47 ± 0.9	47 ± 0.7	47 ± 0.3	48 ± 0.3	32 ± 8.7	47 ± 0.4	47 ± 0.4	47 ± 0.4	50 ± 0.4	50 ± 0.5
Cellulose (%)	30.9 ± 2.7	18.7 ± 3.6	29.9 ± 4.9	13.2 ± 1.6	7.0 ± 1.8	24.8 ± 8.6	30.8 ± 1.8	28.6 ± 2.5	4.8 ± 1.7	7.7 ± 2.5
Klason lignin (%)	33.7 ± 1.8	39.2 ± 3.8	25.7 ± 5.7	45.8 ± 1.1	39.8 ± 8.7	42.7 ± 4.2	36.1 ± 1.4	36.4 ± 2.6	55.7 ± 1.3	55.7 ± 0.3
Ca ($g\ kg^{-1}$)	3.2 ± 2.0	2.1 ± 0.4	1.9 ± 0.6	3.2 ± 0.8	2.2 ± 0.5	1.3 ± 0.3	0.6 ± 0.1	0.7 ± 0.1	1.4 ± 0.2	2.5 ± 1.0
K ($g\ kg^{-1}$)	0.6 ± 0.3	0.5 ± 0.1	< 0.3	0.7 ± 0.1	4.5 ± 1.0	0.4 ± 0.1	0.6 ± 0.4	< 0.3	0.3 ± 0.0	0.4 ± 0.1
Mg ($g\ kg^{-1}$)	0.6 ± 0.4	0.5 ± 0.2	0.3 ± 0.1	0.6 ± 0.1	4.1 ± 1.3	0.4 ± 0.2	0.2 ± 0.0	0.2 ± 0.0	0.2 ± 0.1	0.5 ± 0.2
P ($mg\ kg^{-1}$)	123 ± 29	83 ± 6	< 50	243 ± 15	437 ± 95	87 ± 40	133 ± 85	53 ± 6	100 ± 17	137 ± 21
Fe ($mg\ kg^{-1}$)	97 ± 68	58 ± 22	114 ± 84	408 ± 104	21295 ± 8835	124 ± 66	70 ± 15	94 ± 23	243 ± 67	572 ± 409
Mn ($mg\ kg^{-1}$)	85 ± 78	93 ± 35	36 ± 9	93 ± 49	166 ± 107	107 ± 27	55 ± 17	36 ± 3	60 ± 13	113 ± 35

VS: volatile solids.
EC: electrical conductivity.

2.8. Statistical analyses

The effect of *exposure* (north *vs.* south exposure) and *wood decay stage* (decay classes 1–5) on the chemical parameters and the potential enzymatic activities (except for tripsin-and-papain like protease and palmitate-esterase) was evaluated by a two-factorial analysis of variance (ANOVA). For analysis of the qPCR data, a factorial ANOVA was also carried out in which three factors were fixed: *exposure* (north *vs.* south); *wood decay stage* (decay classes 1–5) and *DNA fraction* (extracellular DNA *vs.* intracellular DNA). The normality and the variance homogeneity of the data were tested prior to ANOVA by using the Shapiro-Wilks and Levene's tests, respectively. Before analysis, data were log- or square root-transformed to meet the assumptions for ANOVA (when it was required). When data did not meet the normality condition, non-parametric tests (Kruskal-Wallis test) were performed to test for differences in wood nutrient content and in the two above-mentioned enzymatic activities (*trip* and *esterpalm*) as a function of exposure and wood decay stage. All the aforementioned analyses were performed with the Statistica software (version 9). Non-metric multidimensional scaling (NM-MDS) on log-normalized data was used to map the physico-chemical parameters to the shifts in microbial abundances (qPCR for both DNA fractions) and enzyme activities at the different wood decay stages as a function of slope exposure. The NM-MDS was calculated based on Bray-Curtis distance indices. The lengths of the arrows indicate the significance of the physico-chemical parameters for sample differentiation. This multivariate analysis was conducted with the PAST software (Version 2.17).

3. Results

3.1. Physico-chemical parameters

An overview of the wood physico-chemical parameters as a function of decay stage (decay classes, DCls 1–5) and exposure (N- *vs.* S-facing slope) is given in Table 3.

Exposure had a significant effect on the moisture content of CWD samples ($F_{1,20} = 17.2$, $p = 0.0005$), with 1.5 times higher values at the N- than at the S-facing slope. An increased moisture level was observed with increasing decay stage ($F_{4,20} = 31.5$, $p \leq 0.0001$), being between 2 and 4 times greater in DCls 4 and 5 than in DCls 1–3 at both slopes. The percentage of volatile solids (VS) was in average 99% for all the decay classes at both slopes, except for DCl 5 at the N-facing slope, where VS were 68%, resulting in a significant interaction between decay class and exposure ($F_{4,100} = 6.2$, $p = 0.002$). Wood pH was significantly affected by the slope exposure ($F_{1,20} = 40.5$, $p \leq 0.0001$), with an average value of 4.0 at the N- and 4.6 at the S-facing site. However, no significant differences were found with respect to the decay stage. At the S-facing site DCls 1, 3 and 4 had 1.5-times higher EC values than at the N-facing site. However, no exposure-effect was found for DCl 2; whilst for DCl 5 EC was 1.5-fold greater at north- than at south exposure (interaction decay class × slope exposure $F_{4,20} = 3.3$, $p = 0.03$). Moreover, twofold lower EC values were recorded in the DCls 3–5 than in DCls 1–2 at the N-facing slope; a decrease in EC with increasing decay stage was also reported at the S-facing site. Although no exposure-effect was detected for the total N content, it differed significantly with the wood decay stage ($p = 0.0001$), with higher values in the DCls 4 and 5 (2–6 times higher) than in the DCls 1–3 at both slopes. In addition, even though the effect of exposure on NH_4^+ content was dependent on the decay class ($F_{4,20} = 24.9$, $p \leq 0.0001$), no clear trend between the N- and the S-facing slopes was detectable. The exposure-effect on the total C content was only evident for the DCl 5 ($p = 0.02$), with a lower amount at the N- than at the S-facing slope. Exposure did not affect the percentage of cellulose ($F_{1,20} = 0.2$, $p = 0.7$); while significant differences were recorded depending on the stage of decay ($F_{4,20} = 40.4$, $p \leq 0.0001$), registering 2- and 4-fold higher values in the DCls 1–3 than in the DCls 4–5. Exposure, however, had a significant impact on the lignin content ($F_{1,20} = 9.5$, $p = 0.006$) being 1.2 times higher at the S- than at the N-facing site, and with greater values for the DCls 4–5 ($F_{4,20} = 6.9$, $p = 0.001$). Ca, K and Mg concentrations were between 2 and 4 times higher at the N-facing slope with respect to the comparable south-facing one ($p = 0.0004$, $p = 0.004$ and $p = 0.002$, respectively). Except for Ca, the concentrations of K and Mg were around 7 times greater in DCl 5 than in DCls 1–4 at north exposure (K: $p = 0.04$; Mg: $p = 0.03$). Exposure did not have a significant effect on P and Fe concentrations; however, both nutrients varied significantly with the stage of decay ($p = 0.0009$ and $p = 0.0003$, respectively), registering the highest P concentration in DCl 5 at both slopes. This decay class was also characterised by a remarkably higher Fe concentration at the N-facing slope, being 52-fold greater than in DCl 4, and between 180 and 360 times higher than in DCls 1–3. Mn concentration was also significantly higher in DCl5 (between 2 and 5 times higher) than in the other decay classes ($p = 0.005$).

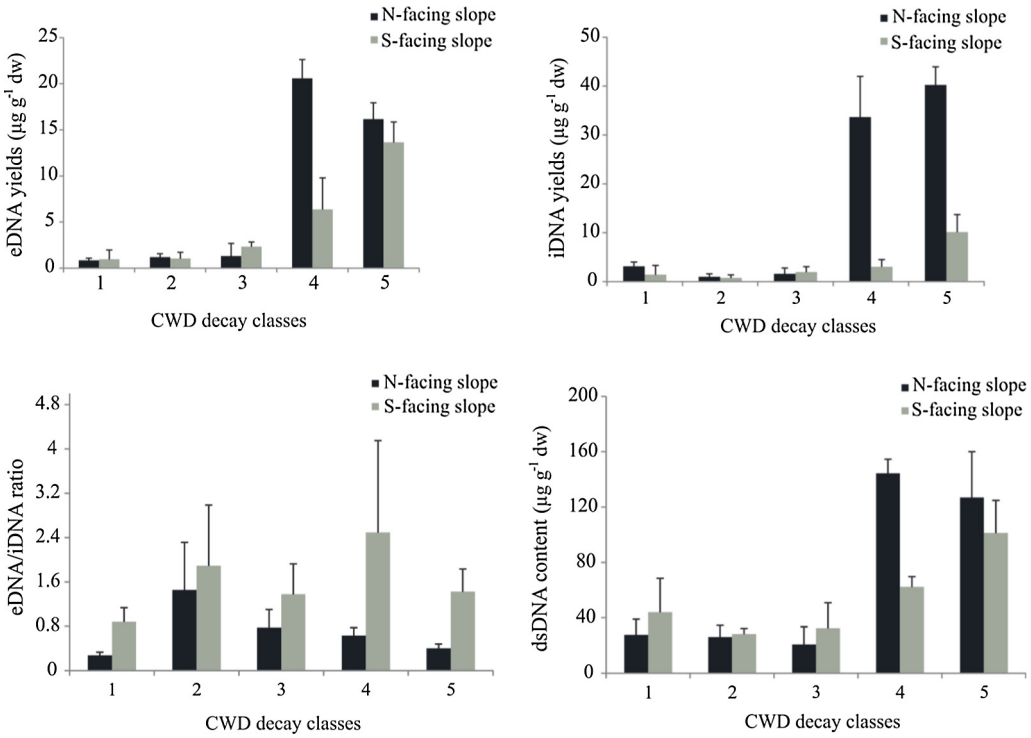

Fig. 1. Yields of extracellular DNA (eDNA; A) and intracellular DNA (iDNA; B); eDNA/iDNA ratio (C); and *ds*DNA content (D) as a function of proceeding decay of *Picea abies* CWD (decay classes 1–5) and slope exposure (north- *vs.* south-facing slope).

3.2. Extra- and intracellular DNA yields

The sequential extraction of the extracellular (eDNA) and intracellular (iDNA) fraction of the total deadwood DNA pool yielded amounts ranging from 1 to 20 μg eDNA g^{-1} wood and from 1 to 40 μg iDNA g^{-1} wood (Fig. 1A, B). Slope exposure significantly influenced the eDNA content only in the case of DCl 4, giving rise to 3-fold higher yields at the N- than at the S-facing slope ($F_{4,20} = 2.8$, $p = 0.04$; Fig. 1A). The stage of decay also had a significant impact on this parameter ($F_{4,20} = 36.1$, $p \leq 0.0001$). At north exposure eDNA content was 17-and 13-times higher in DCls 4 and 5 compared to DCls 1–3; and at south exposure the amount of eDNA was about 6- and 13-fold higher in the last two decay classes, respectively. The exposure-effect on the yields of iDNA was only significant for DCls 4 and 5 ($F_{4,20} = 2.8$, $p = 0.04$; Fig. 1B). The amount of iDNA was 11- and 4-times higher at the N-facing site for these two decay classes (Fig. 1B). In addition, iDNA yields varied significantly with the stage of decay at both slopes ($F_{4,20} = 21.7$, $p \leq 0.0001$), being around 20-times higher in DCls 4 and 5 than in DCls 1–3 at north exposure, while at south exposure it was about 5-fold higher in DCl 5 than in the remaining decay classes (Fig. 1B). A higher eDNA/iDNA ratio was in general found for the CWD samples collected at the S-facing site irrespective of the decay class ($F_{4,20} = 29.0$, $p \leq 0.0001$; Fig. 1C). An exposure-effect on *ds*DNA yields was only recorded for DCl 4, being 2-times higher at the N- than at the S-facing site ($F_{4,20} = 3.1$, $p = 0.04$; Fig. 1D). At both slopes, DCls 4 and 5 had a higher *ds*DNA content (Fig. 1D) in comparison with DCls 1–3 ($F_{4,20} = 23.9$, $p \leq 0.0001$), and these differences were more obvious at north exposure where *ds*DNA yields were around 6-fold higher in the last two decay classes (Fig. 1D).

3.3. Community- and functional gene-level real-time PCR of the extra- and intracellular DNA fractions from P. abies CWD samples

Bacterial abundance was 17- and 3-times higher in CWD samples at the N- than at the S-facing site ($F_{1,100} = 106.1$, $p \leq 0.0001$) for iDNA and eDNA fractions, respectively (Tables 4 and 5). The same trend was observed for fungi ($F_{1,100} = 44.7$, $p \leq 0.0001$) and archaea ($F_{1,100} = 39.7$, $p \leq 0.0001$). Moreover, these three microbial groups were more abundant at the advanced decay stages, i.e., in the DCls 4 and 5 for both DNA fractions, and these differences were more evident at the N-facing slope (bacteria: $F_{4,100} = 6.9$, $p \leq 0.0001$; fungi: $F_{4,100} = 8.4$, $p \leq 0.0001$; archaea: $F_{4,100} = 4.8$, $p = 0.001$). For instance, for the iDNA fraction, the bacterial abundance was 18- and 60-fold higher in the DCls 4 and 5 compared to the DCls 1–3 (Table 5). The same trend was observed for the eDNA fraction in which the abundance of bacteria was 20-times higher in the last two decay classes (Table 4).

CWD samples at the N-facing slope were also characterised by a greater abundance of ammonia-oxidising bacteria (AOB 16S) than those at the S-facing slope irrespective of the decay stage ($F_{1,100} = 158.6$, $p \leq 0.0001$). Moreover, DCls 4 and 5 had the highest AOB 16S abundance with regard to both DNA fractions ($F_{4,100} = 15.4$, $p \leq 0.0001$; Tables 4 and 5). The abundance of *Nitrobacter* sp. followed a similar trend than that shown for AOB 16S (Tables 4 and 5). Exposure also had a significant effect on the *nif*H gene abundance ($F_{1,100} = 131.6$, $p \leq 0.0001$), being 10-fold higher in CWD samples at the N- than at the S-facing slope. Moreover, at north exposure, *nif*H abundance was around 5-fold higher in the advanced decay stages (DCls 4 and 5) than in DCls 1–3 in the eDNA fraction (Table 4); and between 10- and 30-times higher in the iDNA fraction (Table 5). The ammonia-oxidation marker gene *amo*A was studied for targeting both ammonia-oxidising bacteria (AOB) and archaea (AOA). The *amo*A AOB gene was only detected in the iDNA fraction of DCls 4 and 5 at north exposure, reaching values of 4.6×10^5 and 2.3×10^6 copies per gram wood dw, respectively (Table 5). Likewise, at the same slope the *amo*A AOA gene was only detected in the iDNA fraction of DCl 5, having a value of 5.5×10^6 copies per gram wood dw (Table 5). Among the five genera of methanogens, we found that the abundance of *Methanosarcina*, *Methanosphaera* and *Methanoculleus* was below the detection limit (Tables 4 and 5). Nevertheless, the genus

Table 4
Real-time PCR analysis from the extracellular DNA fraction of the decay classes 1–5 from the north- and south-facing slopes. Values are means with standard deviation in brackets. Units are expressed as gene copy number per g wood dry weight.

	North-facing slope					South-facing slope				
Decay classes	1	2	3	4	5	1	2	3	4	5
Bacteria	2.5×10^8 (2.1×10^7)	1.5×10^8 (9.8×10^6)	1.7×10^8 (1.3×10^6)	3.5×10^9 (1.2×10^7)	3.9×10^9 (8.8×10^7)	8.9×10^7 (1.3×10^6)	8.3×10^7 (6.1×10^5)	2.6×10^8 (1.4×10^6)	5.8×10^8 (2.8×10^6)	1.5×10^9 (4.9×10^6)
Fungi	1.7×10^9 (1.5×10^8)	5.8×10^8 (5.8×10^5)	9.2×10^8 (5.7×10^7)	6.3×10^9 (3.6×10^7)	7.3×10^9 (1.9×10^7)	4.4×10^8 (4.8×10^6)	3.9×10^8 (3.4×10^6)	5.9×10^8 (4.6×10^5)	3.9×10^8 (2.1×10^5)	9.5×10^8 (4.7×10^6)
Archaea	1.3×10^8 (1.0×10^6)	9.4×10^7 (4.9×10^6)	1.9×10^8 (1.1×10^7)	1.7×10^9 (1.2×10^7)	8.4×10^8 (3.3×10^6)	1.3×10^8 (1.5×10^6)	6.3×10^7 (6.6×10^5)	6.1×10^7 (3.0×10^5)	6.3×10^7 (2.5×10^5)	2.2×10^8 (1.5×10^5)
AOB16S	7.8×10^6 (7.2×10^4)	1.3×10^7 (1.0×10^5)	1.9×10^7 (1.8×10^5)	3.6×10^7 (3.2×10^5)	2.9×10^7 (2.4×10^5)	6.1×10^6 (1.1×10^4)	5.7×10^6 (1.8×10^5)	6.3×10^6 (1.2×10^5)	8.2×10^6 (5.9×10^4)	2.4×10^7 (3.6×10^5)
Nitrobacter sp.	1.1×10^7 (1.0×10^6)	7.9×10^6 (4.9×10^4)	1.3×10^7 (1.1×10^6)	3.6×10^8 (9.1×10^6)	3.6×10^8 (8.9×10^6)	1.5×10^6 (1.0×10^5)	2.7×10^6 (1.4×10^4)	1.2×10^7 (2.5×10^5)	3.3×10^7 (9.9×10^4)	1.6×10^8 (7.2×10^6)
*nif*H gene	6.3×10^6 (1.2×10^4)	4.8×10^6 (9.8×10^4)	7.0×10^6 (8.3×10^4)	4.2×10^7 (6.4×10^5)	2.9×10^7 (7.9×10^5)	1.4×10^6 (7.9×10^4)	1.1×10^6 (6.8×10^3)	3.9×10^6 (1.4×10^4)	7.5×10^6 (1.0×10^4)	2.3×10^7 (8.4×10^4)
*amo*A-AOB gene	b.d.l.	b.d.l.	b.d.l.	b.d.l.	b.d.l.	b.d.l.	b.d.l.	b.d.l.	b.d.l.	b.d.l.
*amo*A-AOA gene	b.d.l.	b.d.l.	b.d.l.	b.d.l.	b.d.l.	b.d.l.	b.d.l.	b.d.l.	b.d.l.	b.d.l.
Genus *Methanobacterium*	b.d.l.	b.d.l.	1.8×10^6 (8.3×10^5)	b.d.l.	b.d.l.	b.d.l.	b.d.l.	b.d.l.	b.d.l.	b.d.l.
Genus *Methanosaeta*	b.d.l.	b.d.l.	b.d.l.	3.9×10^5 (8.3×10^3)	2.8×10^5 (9.1×10^3)	b.d.l.	b.d.l.	1.3×10^5 (7.2×10^3)	1.8×10^5 (7.6×10^3)	5.3×10^5 (8.2×10^3)

b.d.l. = below detection limit AOB = ammonia-oxidising bacteria AOA = ammonia-oxidising archaea.

Table 5
Real-time PCR analysis from the intracellular DNA fraction of the decay classes 1–5 from the north- and south-facing slopes. Values are means with standard deviation in brackets. Units are expressed as gene copy number per g wood dry weight.

	North-facing slope					South-facing slope				
Decay classes	1	2	3	4	5	1	2	3	4	5
Bacteria	9.6×10^8 (2.2×10^7)	3.7×10^8 (2.1×10^6)	8.4×10^8 (6.5×10^5)	1.1×10^{10} (2.8×10^6)	3.7×10^{10} (3.6×10^6)	3.1×10^8 (3.1×10^6)	1.3×10^8 (1.2×10^6)	2.4×10^8 (1.3×10^6)	6.2×10^8 (4.8×10^5)	1.7×10^9 (4.3×10^6)
Fungi	1.9×10^9 (1.6×10^6)	2.2×10^9 (1.5×10^6)	1.5×10^9 (1.4×10^3)	1.4×10^{10} (7.6×10^6)	1.0×10^{10} (2.2×10^6)	7.9×10^8 (5.2×10^5)	2.4×10^9 (7.2×10^6)	2.4×10^9 (9.8×10^6)	2.6×10^9 (7.8×10^6)	6.1×10^9 (1.0×10^6)
Archaea	1.3×10^8 (1.0×10^6)	9.4×10^7 (4.9×10^5)	2.0×10^8 (1.1×10^4)	1.7×10^9 (1.2×10^6)	8.4×10^8 (3.3×10^6)	1.3×10^8 (1.8×10^5)	6.3×10^7 (1.1×10^4)	6.1×10^7 (3.0×10^4)	6.3×10^7 (2.5×10^4)	2.2×10^8 (9.8×10^5)
AOB16S	9.1×10^6 (1.4×10^3)	1.8×10^7 (6.3×10^4)	1.9×10^7 (1.1×10^4)	4.4×10^7 (4.9×10^4)	9.7×10^7 (7.2×10^5)	7.2×10^6 (3.4×10^3)	6.9×10^6 (9.4×10^4)	6.3×10^6 (8.8×10^3)	8.8×10^6 (2.4×10^3)	2.5×10^7 (5.9×10^4)
Nitrobacter sp.	4.3×10^7 (4.2×10^4)	9.0×10^6 (6.7×10^4)	4.9×10^7 (4.8×10^5)	7.9×10^8 (2.3×10^5)	1.9×10^9 (1.1×10^5)	1.8×10^7 (2.1×10^4)	8.7×10^6 (6.1×10^3)	1.5×10^7 (4.1×10^3)	5.4×10^7 (4.4×10^3)	1.8×10^8 (5.5×10^4)
*nif*H gene	7.5×10^6 (9.3×10^3)	1.1×10^7 (7.3×10^5)	2.7×10^7 (9.5×10^4)	2.3×10^8 (1.1×10^5)	2.6×10^8 (7.6×10^5)	7.1×10^6 (1.3×10^3)	1.5×10^6 (8.8×10^3)	3.9×10^6 (9.9×10^3)	1.1×10^7 (6.8×10^3)	2.7×10^7 (1.1×10^4)
*amo*A-AOB gene	b.d.l.	b.d.l.	b.d.l.	4.6×10^5 (1.3×10^3)	2.3×10^6 (7.3×10^3)	b.d.l.	b.d.l.	b.d.l.	b.d.l.	b.d.l.
*amo*A-AOA gene	b.d.l.	b.d.l.	b.d.l.	b.d.l.	5.5×10^6 (8.1×10^3)	b.d.l.	b.d.l.	b.d.l.	b.d.l.	b.d.l.
Genus *Methanobacterium*	b.d.l.	b.d.l.	7.1×10^6 (9.3×10^3)	2.6×10^5 (1.0×10^3)	1.9×10^5 (9.3×10^3)	b.d.l.	b.d.l.	b.d.l.	b.d.l.	b.d.l.
Genus *Methanosaeta*	b.d.l.	b.d.l.	b.d.l.	1.9×10^6 (5.3×10^3)	3.4×10^6 (8.2×10^3)	b.d.l.	b.d.l.	2.6×10^5 (9.3×10^2)	4.0×10^5 (1.3×10^2)	2.7×10^6 (7.8×10^3)

b.d.l. = below detection limit.
AOB = ammonia-oxidising bacteria.
AOA = ammonia-oxidising archaea.

Methanobacterium was detected in the iDNA fraction of the DCls 3–5 (Table 5), and in the eDNA fraction of the DCl 3 at the N-facing site (Table 4). In addition, at both slopes the genus *Methanosaeta* was present in both DNA fractions of the DCls 4 and 5 (Tables 4 and 5).

3.4. Potential enzymatic activities

An overview of the potential hydrolytic enzyme activities from CWD samples at the different decay stages and exposure is given in Table 6. DCls 4 and 5 showed a higher arylsulphatase activity at the N- than at the S-facing slope (9 and 3-times higher, respectively); however, no significant exposure-effects were found for DCls 1–3 (exposure x decay class $F_{4,20} = 3.34$, $p = 0.03$). The exposure-effect on chitinase activity was also dependent on the decay class ($F_{4,20} = 2.95$, $p = 0.04$), with greater values (2 and 4 times) at the N-facing slope for DCls 1 and 4. However, a higher leucine-aminopeptidase activity was recorded at the S-facing slope, except for DCl 4 which showed a higher activity (3 times) at the N-facing site ($F_{4,20} = 2.89$, $p = 0.04$). In contrast, exposure did not have a significant impact on the tripsin-and papain-like protease activity. The stage of wood decay affected significantly these two latter enzyme activities (*leu*: ANOVA $F_{4,20} = 4.3$; $p = 0.01$; *trip*: Kruskal-Wallis test $H_{4,30} = 21.6$; $p = 0.0002$). At north exposure the highest activities were registered for DCl 4; while at south exposure the highest levels were detected in DCls 3 and 5 for leucine-aminopeptidase and tripsin-and papain-like protease activities, respectively.

The potential activities of α- and β-glucosidases, cellulase and xylanase also varied significantly with exposure and decay stage (*alfaG*: $F_{4,20} = 4.3$, $p = 0.002$; *betaG*: $F_{4,20} = 4.8$, $p = 0.007$; *cell*: $F_{4,20} = 4.9$, $p = 0.006$; *xil*: $F_{4,20} = 4.6$, $p = 0.009$). The same trend

Table 6
Potential enzymatic activities in the decay classes 1–5 from the north- and south-facing slopes. The full name of the enzymatic activities is given in Table 2. Values are means ± standard deviation. Data are expressed as nanomoles of MUF min^{-1} g^{-1} wood dry weight.

	North-facing slope					South-facing slope				
Decay classes	1	2	3	4	5	1	2	3	4	5
aryS	1.9 ± 1.1	1.7 ± 0.2	1.8 ± 0.9	20.5 ± 7.1	38.5 ± 13.4	1.3 ± 0.9	1.5 ± 0.4	1.4 ± 0.1	2.2 ± 1.4	13.3 ± 5.3
chit	93.3 ± 53.1	46.4 ± 10.8	31.4 ± 14.3	51.1 ± 24.3	16.2 ± 8.3	38.1 ± 13.5	41.3 ± 9.8	42.2 ± 14.4	11.6 ± 8.7	15.5 ± 5.4
leu	31.3 ± 14.9	25.3 ± 10.7	44.2 ± 19.5	248.6 ± 39.4	67.6 ± 28.0	54.7 ± 39.6	75.1 ± 32.1	204.6 ± 74.7	88.0 ± 10.8	119.6 ± 40
trip	0.0 ± 0.0	0.3 ± 0.02	0.2 ± 0.01	3.2 ± 0.4	0.8 ± 0.1	0.0 ± 0.0	0.0 ± 0.0	0.0 ± 0.0	0.5 ± 0.08	1.1 ± 0.4
alfa_G	3.3 ± 1.3	0.8 ± 0.05	2.0 ± 0.9	9.0 ± 2.3	2.4 ± 0.9	1.6 ± 0.9	1.5 ± 0.4	2.0 ± 0.6	2.6 ± 0.9	2.1 ± 1.0
beta_G	202.5 ± 91.6	41.3 ± 3.7	42.9 ± 13.0	381.1 ± 72.8	93.7 ± 9.9	89.5 ± 35.4	83.5 ± 36.3	114.3 ± 25.6	159.0 ± 36.7	118.6 ± 57.3
cell	34.9 ± 14.2	3.8 ± 1.1	3.5 ± 1.9	73.3 ± 29.3	11.2 ± 1.0	16.5 ± 12.6	14.3 ± 6.3	18.0 ± 8.0	18.0 ± 2.9	14.2 ± 8.2
xil	16.9 ± 9.1	5.0 ± 1.0	9.2 ± 3.1	66.7 ± 10.3	19.3 ± 5.7	10.6 ± 2.3	15.7 ± 7.0	20.8 ± 4.5	28.3 ± 5.3	22.7 ± 9.5
uroni	1.3 ± 0.7	0.8 ± 0.1	0.7 ± 0.3	7.7 ± 2.1	3.9 ± 1.3	1.3 ± 0.5	1.8 ± 0.8	2.5 ± 1.3	3.4 ± 0.6	4.8 ± 2.3
ester_ac	1956 ± 943	1354 ± 243	1026 ± 333	5224 ± 1639	2958 ± 1629	1483 ± 699	1528 ± 448	1969 ± 349	2933 ± 714	2788 ± 416
ester_nona	144.1 ± 24.7	36.2 ± 10.0	53.8 ± 17.9	1465 ± 761	294 ± 87	131.8 ± 43.3	91.7 ± 38.0	131.9 ± 55.1	244.4 ± 53.4	214.0 ± 64.1
ester_palm	1.4 ± 0.9	0.2 ± 0.01	0.2 ± 0.05	4.8 ± 1.9	1.3 ± 0.3	0.2 ± 0.05	0.1 ± 0.02	0.3 ± 0.03	0.4 ± 0.01	0.7 ± 0.09
acP	160.8 ± 43.1	35.2 ± 12.3	282.4 ± 97.2	1339 ± 337.5	1514 ± 517	134.9 ± 25.3	185.6 ± 30.9	467.4 ± 95.4	960.1 ± 312	1476 ± 515
bisP	11.2 ± 5.9	2.4 ± 0.9	19.8 ± 13.3	33.4 ± 6.8	18.5 ± 6.1	10.0 ± 3.7	6.4 ± 1.8	12.1 ± 3.8	15.9 ± 5.9	28.7 ± 6.9
piroP	1.1 ± 0.2	0.4 ± 0.05	4.9 ± 1.7	4.2 ± 1.5	2.3 ± 0.8	0.6 ± 0.07	0.5 ± 0.04	0.5 ± 0.1	1.3 ± 0.08	2.9 ± 0.9
inosit	7.0 ± 1.1	1.6 ± 0.6	7.5 ± 3.3	16.5 ± 1.6	11.3 ± 4.6	3.2 ± 1.2	4.6 ± 1.8	9.4 ± 3.1	13.8 ± 4.9	13.7 ± 4.7
alkP	35.0 ± 14.4	0.7 ± 0.1	22.5 ± 6.6	119.3 ± 59.2	45.4 ± 27.7	13.2 ± 2.9	11.2 ± 4.0	23.3 ± 13.7	50.4 ± 14.4	90.6 ± 20.7

was observed for glucuronidase, acetate esterase and palmitate esterase activities (*uroni*: $F_{4,20} = 12.3$, $p \leq 0.0001$; *esterac*: $F_{4,20} = 8.6$, $p = 0.0003$; *esterpalm*: Kruskal-Wallis test $H_{4,30} = 10.8$; $p = 0.03$). In addition, at the N-facing slope the highest activities were in general recorded for the DCl4.

No exposure-effect was found for any of the enzymes involved in the P-cycle. Nonetheless, they were significantly influenced by the stage of wood decay (*acP*: $F_{4,20} = 35.3$, $p \leq 0.0001$; *alkP*: $F_{4,20} = 7.1$, $p = 0.001$; *bisP*: $F_{4,20} = 7.7$, $p = 0.0006$; *inosit*: $F_{4,20} = 8.1$, $p = 0.0005$), with the exception of pyrophosphate-phosphodiester ase. Higher activities were in general recorded in DCls 4 and 5 than in DCls 1–3.

3.5. Non-metric multidimensional scaling (NM-MDS) analysis

Exposure effects and the physico-chemical parameters shaping the microbiological properties (microbial abundances and enzyme activities) from *Picea abies* CWD at different decay stages were visualised in the NM-MDS plot (Fig. 2). Overall, DCls 1–3 (negative side) grouped differently from DCls 4 and 5, which were found to cluster on the positive side of the first ordination axis, indicating that each decay class, independently of the slope exposure, represents a special matrix and thus, a specific microhabitat. Moisture ($r = 0.77$) along with N, P and Fe contents ($r = 0.87$, 0.72 and 0.73) were the major determinants for the clustering of the CWD samples along this axis, with higher values with increasing stage of decay. The opposite trend was observed for EC, that it was negatively correlated with axis 1 ($r = -0.72$). Moreover, CWD samples were differentiated along the second axis as a function of exposure, with N-facing samples at the positive side and S-facing ones at the negative side, being pH the most important parameter ($r = 0.44$) for this differentiation.

3.6. X-ray tomography

X-ray microtomography (μCT) analyses enabled the differentiation of the wood cell types, including tracheids, vessels, xylem rays and bordered pits, as a function of slope exposure and decay stage (Figs. 3–6). Generally, no substantial differences were detected among the first three decay classes (DCls 1–3). On the one hand, no sign of degradation was in general observed for the tracheid cell walls of the DCl 1 (Figs. 3 and 4). Nonetheless, the degradation of the wood cell wall was evident for the DCl 4, being this fact more pronounced at the N-facing slope (*data not shown*); indeed, the structure of the xylem rays showed signs of degradation only for the CWD samples collected at this slope. The DCl 5 was even more degraded than DCl4 showing cracks along the radial direction (Figs. 5 and 6). Furthermore, if we consider the tangential 3D view, the bordered pits in the DCl5 could only be distinguished at the S-facing slope (Fig. 6), indicating a higher degree of physical cell damage at north exposure.

In addition, the details of the pit structure were easily observed for the DCl 1 (Figs. 3 and 4), in which the pit torus (with both walls easily discernible) and the aperture were visible. For DCls 2 and 3 the details of the pit torus were visible (*data not shown*), although not as easily distinguishable as for DCl 1. However, for the DCls 4 and 5, the pit torus was not visible probably due to physical cell damage, and therefore we could only see the corresponding apertures with a bigger diameter (Fig. 5 and 6).

4. Discussion

North-facing slopes are generally cooler than comparable south-facing ones (Egli et al., 2006, 2009), but unexpectedly higher microbial abundances were revealed by qPCR in *Picea abies* CWD samples at north exposure irrespective of the decay class and for all of the three microbial domains (bacteria, fungi and archaea). However, in the same study area and for soil microbial communities, Bardelli et al. (2016) observed that the exposure-effect was domain-specific: bacteria (S > N, altitude-independent); fungi (N ∼ S); and archaea (N > S, altitude-dependent). Furthermore, in the present study higher abundances of some selected microbial parameters related to the N-cycle (AOB 16S, *Nitrobacter* sp. and nitrogen fixers *nifH*) were recorded at the north- than at the south-facing slope regardless of the decay class. This thermal signal related to exposure was also evident for the *amo*A gene, as the gene copy numbers for both AOB and AOA were only detected at the north-facing site for the advanced decay stages (DCls 4 and 5). The same trend was observed for the genus *Methanobacterium*. These exposure-effects and, in general, the climate impact on the wood-inhabiting microbiota are of great relevance with regard to the functioning of forest ecosystems because on the one hand, AOA and AOB are responsible for ammonia oxidation, the first and rate limiting step in the process of nitrification (Wessén and Hallin, 2011); and, on the other hand, the detection of methanogenic archaea (*Methanobacterium and Methanosaeta)* in the latest decay stages suggests that woody debris might act as a source of

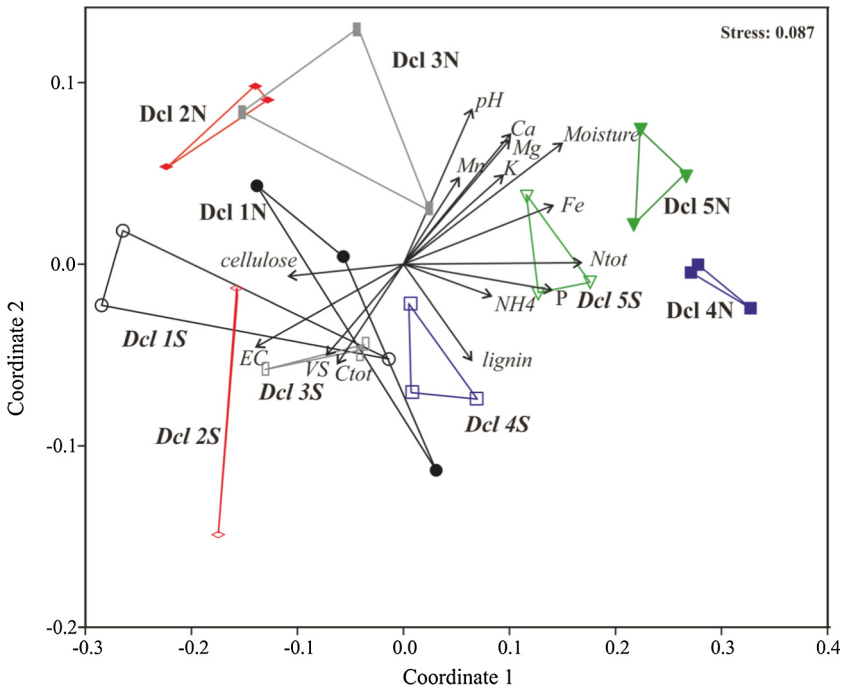

Fig. 2. Non-metric multidimensional scaling (NM-MDS) on log-normalized data was used to map the physico-chemical parameters to the shifts in microbial abundances for both DNA fractions (eDNA and iDNA) assessed by real-time PCR and enzyme activities at the different wood decay stages as a function of slope exposure. The NM-MDS was calculated based on Bray-Curtis distance indices. The lengths of the arrows indicate the significance of the physico-chemical parameters for sample differentiation. The different colored triangles refer to the different decay classes (DCl 1: black; DCl 2: red; DCl3: grey; DCl4: blue; and DCl5: green). Full and empty symbols refer to the north- and the south-facing slope respectively. (For interpretation of the references to colour in this figure legend, the reader is referred to the web version of this article.)

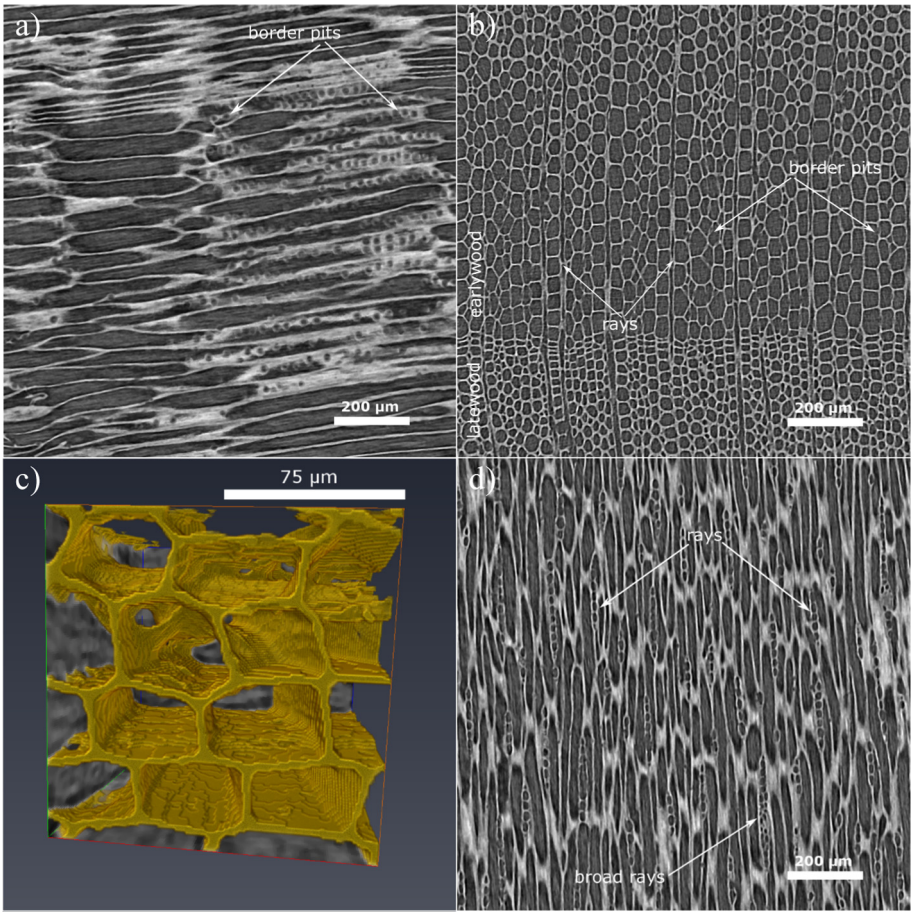

Fig. 3. Structure of the decay class 1, north-facing slope obtained by X-ray tomography analyses: a – tangential view, b – longitudinal view, c – 3D visualization of a 150 × 150 × 150 voxels sub-volume, d – radial view.

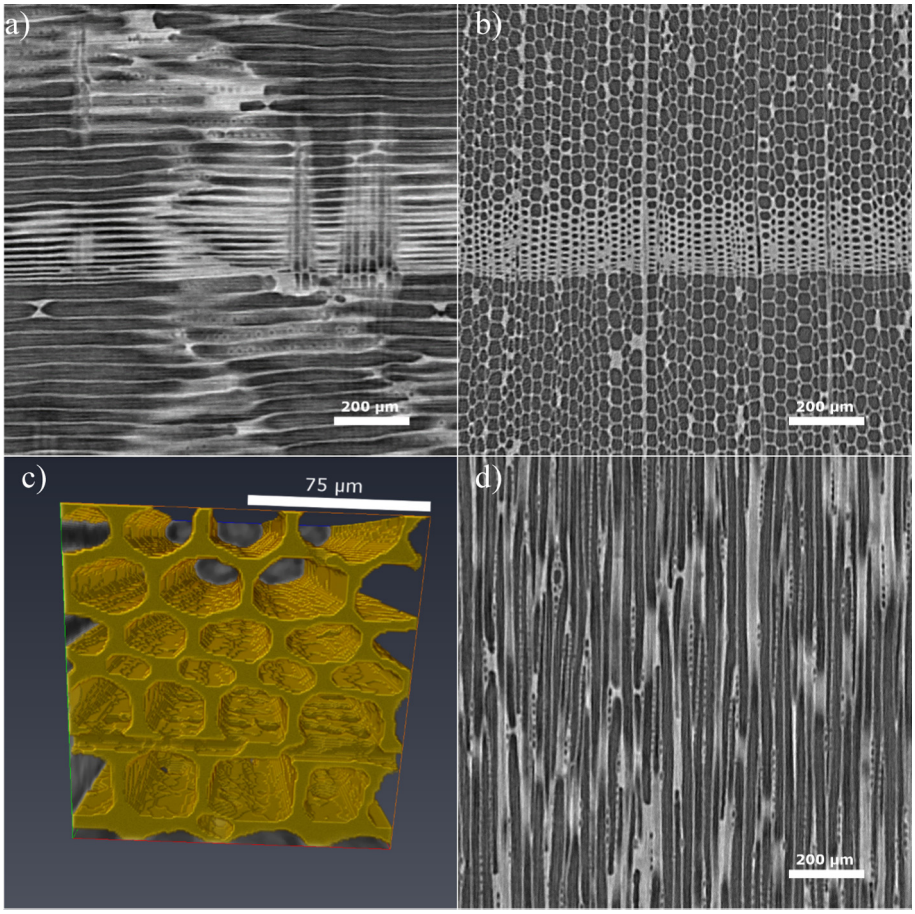

Fig. 4. Structure of the decay class 1, south-facing slope obtained by X-ray tomography analyses: a – tangential view, b – longitudinal view, c – 3D visualization of a 150 × 150 × 150 voxels sub-volume, d – radial view.

biogenic methane, the second most important anthropogenic greenhouse gas after CO_2, as previously reported by Mukhin and Voronin (2007, 2009). These authors proposed a symbiotic association between wood-degrading fungi and methanogenic archaea, where fungi cleave wood carbohydrates and lignin and the products formed are fermented to produce carbon dioxide and hydrogen, the substrates for methane.

In accordance with the qPCR findings, we observed that the content of certain nutrients (Ca, K and Mg) was also greater in the CWD samples from the north- than those from the south-facing sites. This is a consequence of the larger availability of these nutrients in the soil from the north-facing slope, which could lead to a higher nutrient richness in the *P. abies* tissues and in turn, in the debris at this slope. This is probably related to the higher moisture level and clay content (linked to the higher weathering of the soils) along with the lower pH level at the north-facing sites (Fravolini et al., 2016), which are favourable conditions especially for fungal wood decomposers. Soil moisture controls nutrient availability and oxygen diffusion required for microbial decomposition (Herrmann and Bauhus, 2012) and influences therefore largely the deadwood decomposition rates.

Furthermore, enzyme-specific exposure effects were recorded for *P. abies* CWD samples even though this thermal signal (N *vs.* S) was strongly dependent on the decay class for most of the enzymes. However, none of the enzymatic activities involved in the P-cycle varied with exposure irrespective of the stage of wood decay. To avoid misinterpretation of environmental changes induced effects a multiple enzyme assay is, therefore, strongly recommended (Bardelli et al., 2016). There is a common acceptance that wood moisture is one of the major factors shaping enzyme activities (Baldrian et al., 2010; van der Wal et al., 2015). We also found that microbial biomass (using *ds*DNA), together with the yields of intracellular DNA (iDNA; potential living microbiota), positively correlated with most of the enzymes (*data not shown*) indicating that iDNA makes up the quantitatively dominant portion of the deadwood DNA pool as previously observed in soil (Ascher et al., 2009).

Among the studied wood properties, pH was the most influential driving factor. For soils it has also been shown that even small variations of pH may induce changes in the microbial abundance and diversity, primarily for bacteria (Bardelli et al., 2016; Lauber et al., 2009). Hoppe et al. (2015b) assumed that variations in the abundances of bacterial phyla are rather determined by a combination of wood properties (i.e., C and N concentration, relative wood moisture, density) than by single parameters, such as pH, alone. Baldrian et al. (2016) reported that pH, together with the lignin content, are the best predictors for enzyme activity in coarse deadwood of *P. abies*, *Abies alba* and *Fagus sylvatica* in a mixed natural temperate forest.

The *eDNA*/*iDNA* ratio was used as an indicator of microbial activity of the wood decomposing microbiota. As expected, lower ratios, indicative of higher microbial activity, were found in the CWD samples at the north-facing site. This could be due to a higher degradation of eDNA (due to enzymatic digestion and consumption as microbial nutrient) and/or to higher iDNA yields at the north-facing slope. This suggests a higher occurrence of living wood-inhabiting microbiota at this slope probably due to the more favourable conditions (i.e., higher moisture and higher nutrient

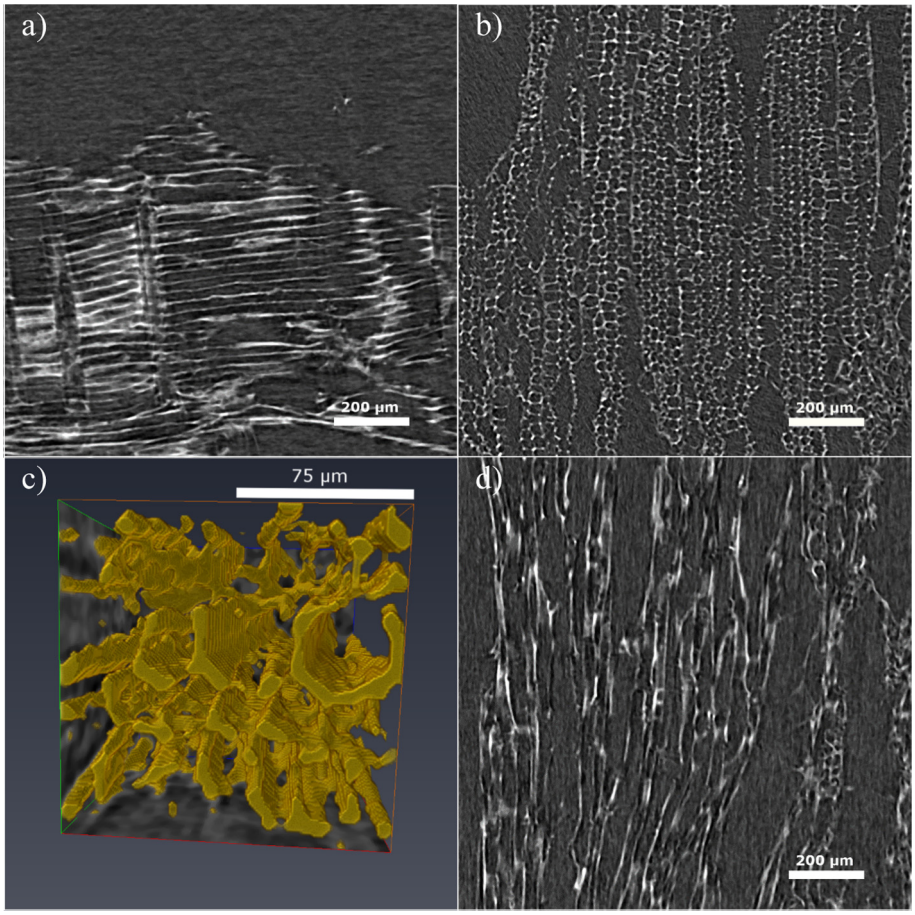

Fig. 5. Structure of the decay class 5, north-facing slope obtained by X-ray tomography analyses: a – tangential view, b – longitudinal view, c – 3D visualization of a 150 × 150 × 150 voxels sub-volume, d – radial view.

contents). These findings are supported by higher microbial abundances (qPCR) registered at the cooler and moister north-facing slope.

As a function of progressing decay, higher eDNA yields were recorded for the latest stages (DCls 4 and 5) at both slopes. The same trend was observed for both the *ds*DNA and the iDNA yields. As a result, higher microbial abundances prevailed in the last two decay classes. However, the *eDNA*/*iDNA* ratio did not show a clear trend with progressing wood decay. The increased amount of eDNA in the last two decay stages is probably due to the release of DNA into the extracellular environment as a consequence of cell death (higher microbial turnover rate). Despite the fact that DNA may act as a source of easily available micronutrients, in our study the higher amounts of micronutrients present at the most advanced stages of decay appear to have been sufficient to satisfy the microbial nutrient demand. However, at the earlier stages of decay where nutrients are more limited, microbes are thought to preferentially feed on eDNA, and consequently lower amounts of eDNA were registered in the first three decay classes.

In comparison to litter, leaves and needles, CWD is a nutrient-poor substrate (Vestin et al., 2013). The elemental nutrient contents usually increase with increasing decay stage (Bütler et al., 2007: *P. abies*, Swiss Jura Mountains; Petrillo et al., 2015, 2016: *P. abies, Larix decidua*, Trentino; Lombardi et al., 2013: *Abies alba* and *Fagus sylvatica*, Apennines). This could be due to respiratory C losses (Petrillo et al., 2015) and/or to an active nutrient transfer from the forest floor by mycelial cords of wood-decaying fungi. Accordingly, the highest concentration for most of the nutrients (except for Ca) was detected in the decay class 5. These differences among decay classes were more evident at north exposure, in particular for Fe. In fact, the NM-MDS analysis pointed out Fe as the most important micronutrient together with N and P for grouping the CWD samples according to their stage of decay. Iron is an important structural component of lignin peroxidases (LiP) that are heme-containing glycoproteins present in white-rot fungi with a central role in the biodegradation of lignin in wood decay processes (Dashtban et al., 2010). Unlike the other peroxidases, LiP enzymes are able to oxidise non-phenolic aromatic substrates and do not require the participation of mediators due to its unusually high redox potential (Dashtban et al., 2010). Nitrogen is a limited nutrient in early wood decay and can be accumulated over time (Baldrian et al., 2016). The importance of nitrogen for fungi relies on the fact that it is required for the chitin cell wall, for proteins, lipids (e.g. sphingolipids) and nucleic acids (Purahong et al., 2016). Through their hyphae, fungi can access nitrogen pools in the surrounding soil and transport it to their deadwood habitat. Merrill and Cowling (1966) along with Larsen et al. (1978) suggested that associations with diazotrophic bacteria might enable fungi to overcome their N deficiencies and they showed that N fixation takes place in living sporocarps. In accordance with these pioneering studies, Hoppe et al. (2014) found positive correlations between fungal sporocarps and the richness of *nifH* (dinitrogen reductase) genes in deadwood logs from *Fagus sylvatica* and *P. abies*. We also observed that *nifH* was strongly correlated with the fungal abundance with respect to the eDNA fraction ($R = 0.90$, $p < 0.001$) at the north-facing site. At this slope and concerning the iDNA fraction, the interaction between *nifH* and fungi was close to the significance level ($R = 0.51$, $p = 0.05$). At south exposure and for iDNA

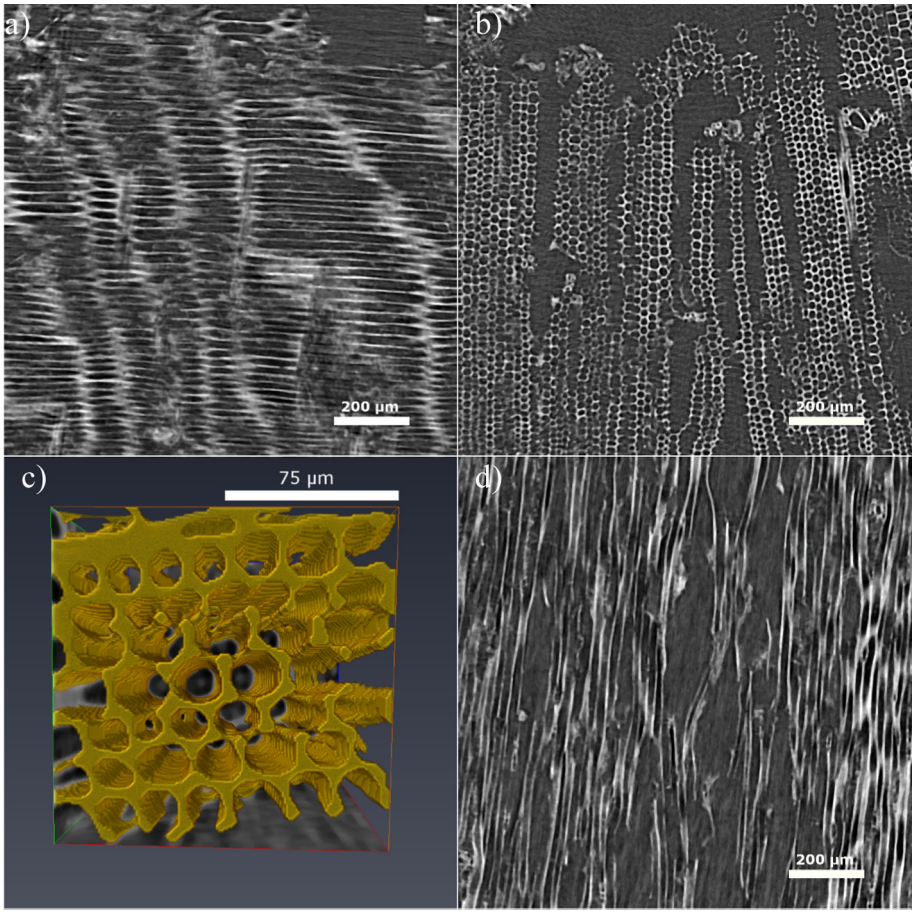

Fig. 6. Structure of the decay class 5, south-facing slope obtained by X-ray tomography analyses: a – tangential view, b – longitudinal view, c – 3D visualization of a 150 × 150 × 150 voxels sub-volume, d – radial view.

there was also a significant correlation between these two microbial groups (R = 0.69, p = 0.004). All in all, this points to the existence of potential fungal-bacterial interactions in wood, even though, as recently reviewed by Johnston et al. (2016), further research is necessary to unravel the exact identity of such associations (mutualism, commensalism or parasitism), and the major abiotic and biotic factors driving these interactions during wood decay.

Our "decay class - DNA - qPCR approach" confirmed Hunter's five decay-class system of being capable of tracing back the different decay stages of *Picea abies* CWD in subalpine Italian forests. Cellulose concentrations were depleted as a function of progressing decay which is in agreement with previous studies (Bütler et al., 2007; Petrillo et al., 2015, 2016). This can be explained by a preferential degradation of cellulose by brown rot fungi (Lombardi et al., 2013). In contrast, the lignin content increased with progressing decay due to its slower degradation and therefore passive enrichment in the remaining deadwood (Petrillo et al., 2015). Fravolini et al. (2016) observed that almost no time trend was detectable for lignin, while the mass of deadwood and cellulose exhibited a continuous loss during a 2-year mesocosm study on *P. abies*-wood blocks under controlled field conditions in the Trentino area.

The high-resolution X-ray microtomography, capable of non-invasive determination and three-dimensional visualization of the wood structure as recently reviewed by Brodersen (2013), permitted to trace back the various stages of *P. abies* deadwood decay. Wood is a complex anisotropic biomaterial and its decay induces significant structural changes, modifying its physico-mechanical properties (Sedighi Gilani et al., 2014). In fact, we observed a higher degree of physical cell damage and disruption at the advanced decay stages (DCls 4 and 5), mainly at the cooler and moister north-facing site characterised by a higher fungal abundance. Fungal deadwood decay involves the initial degradation of the cell wall components through the release of cell penetrating agents that favour the enzymes entrance, which can cause a significant damage to the wood structure (Sedighi Gilani et al., 2014; Thybring, 2013).

5. Conclusions

The common five decay-class system in combination with the eDNA *vs.* iDNA approach offered the possibility to trace back the decay stages of *Picea abies* CWD under different climatic conditions in mountain forest ecosystems. Our findings underline the importance of a multifactorial approach to understand deadwood decomposition, encompassing both physico-chemical and microbiological methods. In disagreement with our first hypothesis, decomposition of *P. abies* deadwood was enhanced at the cooler, more acidic and moister north-facing slope that offered more favourable conditions especially for fungi. As expected, these exposure-effects (N > S) on microbial abundances were in general more evident for the advanced decay stages (DCls 4 and 5); while for most of the enzymatic activities the impact of exposure was enzyme-specific and strongly dependent on the decay class. Our third hypothesis was partially corroborated since a lower eDNA/iDNA ratio, indicative of a higher microbial activity, was found at

the north-exposure, in line with the higher physical wood damage shown by the X-ray microtomography at this slope. In contrast to our expectations, however, this ratio did not show a clear trend with progressing wood decay. Further studies are needed to unravel the taxonomic identities and genomic potential of bacterial wood decomposers and their interactions with wood decaying fungi. To conclude, our findings confirmed that deadwood at the advanced stages of decomposition act as *hot spot* for microbial life.

Acknowledgements

M. Gómez-Brandón and J. Ascher-Jenull have been funded by the Fonds zur Förderung der Wissenschaftlichen Forschung (FWF) Austria (Project I989-B16). J. Ascher-Jenull has also been partially funded by the Ente Cassa di Risparmio di Firenze (Florence, Italy). Tommaso Bardelli has been funded by a PhD grant (DT16364) from the University of Florence (Italy). We would like to thank Marta Petrillo and Rebecca Mayer for their help in the field sampling. We are also indebted to Dr. Fabio Angeli of the *Ufficio distrettuale forestale* – Malé (Trento, Italy) and his team for their support in the field. We acknowledge Paul Fraiz for his highly valuable help in language editing.

References

Ascher, J., Ceccherini, M.T., Pantani, O.L., Agnelli, A., Borgogni, F., Guerri, G., Nannipieri, P., Pietramellara, G., 2009. Sequential extraction and genetic fingerprinting of a forest soil metagenome. Appl. Soil Ecol. 42, 176–181.

Ascher, J., Sartori, G., Graefe, U., Thornton, B., Ceccherini, M.T., Pietramellara, G., Egli, M., 2012. Are humus forms, mesofauna and microflora in subalpine forest soils sensitive to thermal conditions? Biol. Fertil. Soils 48, 709–725.

Baldrian, P., Merhautová, V., Petránková, M., Cajthaml, T., Šnajdr, J., 2010. Distribution of microbial biomass and activity of extracellular enzymes in a hardwood forest soil reflect soil moisture content. Appl. Soil Ecol. 46, 177–182.

Baldrian, P., Zrustova, P., Tláskal, V., Davidova, A., Merhautová, V., Vrška, 2016. Fungi associated with decomposing deadwood in a natural beech- dominated forest. Fungal Ecol. 23, 109–122.

Bardelli, T., Gómez-Brandón, M., Ascher-Jenull, J., Fornasier, F., Arfaioli, P., Francioli, D., Egli, M., Sartori, G., Insam, H., Pietramellara, G., 2016. Effects of slope exposure on soil physico-chemical and microbiological properties along an altitudinal climosequence in the Italian Alps. Sci. Total Environ.

Boettger, T., Haupt, M., Knoller, K., Weise, S.M., Waterhouse, J.S., Rinne, K.T., Loader, N.J., Sonninen, E., Jungner, H., Masson-Delmotte, V., Stievenard, M., Guillemin, M.T., Pierre, M., Pazdur, A., Leuenberger, M., Filot, M., Saurer, M., Reynolds, C.E., Helle, G., Schleser, G.H., 2007. Wood cellulose preparation method and mass spectrometric analysis of delta C-13, delta O-18, and nonexchangeable delta H-2 values in cellulose, sugar and starch: An interlaboratory comparison. Anal. Chem. 79, 4603–4612.

Bradford, M.A., Ii, R.J.W., Baldrian, P., Crowther, T.W., Maynard, D.S., Oldfield, E.E., Wieder, W.R., Wood, S.A., King, J.R., 2014. Climate fails to predict wood decomposition at regional scales. Nat. Clim. Chang. 4, 625–630.

Brodersen, C.R., 2013. Visualizing wood anatomy in three dimensions with high-resolution X-ray micro-tomography (MCT) – a review. IAWA J. 34, 408–424.

Bütler, R., Patty, L., LeBayon, R., Guenat, C., Schlaepfer, R., 2007. Log decay of *Picea abies* in the Swiss Jura Mountains of central Europe. Forest Ecol. Manage. 242, 791–799.

Coolen, M.J.L., Hopmans, E.C., Rijpstra, W.I.C., Muyzer, G., Schouten, S., Volkman, J.K., Sinninghe Damsté, J.S., 2004. Evolution of the methane cycle in Ace Lake (Antarctica) during the Holocene: response of methanogens and methanotrophs to environmental change. Org. Geochem. 35, 1151–1167.

Dashtban, M., Schraft, H., Syed, T.A., Qin, W., 2010. Fungal biodegradation and enzymatic modification of lignin. Int. J. Biochem. Mol. Biol. 1, 36–50.

De Boer, W., Van der Wal, A., 2008. Interactions between saprotrophic basidiomycetes and bacteria. In: Boddy, L., Frankland, J.C., Van West, P. (Eds.), Ecology of Saprotrophic Basidiomycetes. Academic Press, Amsterdam, pp. 142–151.

Dence, C.W., Lin, S.Y., 1992. Methods in Lignin Chemistry. Springer, Heidelberg.

Egli, M., Mirabella, A., Sartori, G., Zanelli, R., Bischof, S., 2006. Effect of north and south exposure on weathering rates and clay mineral formation in Alpine soils. Catena 67, 155–174.

Egli, M., Sartori, G., Mirabella, A., Favilli, F., 2009. Effect of north and south exposure on organic matter in high Alpine soils. Geoderma 149, 124–136.

Ferris, M.J., Muyzer, G., Ward, D.M., 1996. Denaturing gradient gel electrophoresis profiles of 16S rRNA-defined populations inhabiting a hot spring microbial mat community. Appl. Environ. Microbiol. 62, 340–346.

Fischer, A.L., Moncalvo, J.-M., Klironomos, J.N., Malcolm, J.R., 2012. Fruiting body and molecular rDNA sampling of fungi in woody debris from logged and unlogged boreal forests in northeastern Ontario. Ecoscience 19, 374–390.

Floudas, D., Binder, M., Riley, R., Barry, K., Blanchette, R.A., Henrissat, B., Martínez, A. T., Otillar, R., Spatafora, J.W., Yadav, J.S., et al., 2012. The Paleozoic origin of enzymatic lignin decomposition reconstructed from 31 fungal genomes. Science 336, 1715–1719.

Folman, L.B., Gunnewiek, P.J.K., Boddy, L., de Boer, W., 2008. Impact of white-rot fungi on numbers and community composition of bacteria colonizing beech wood from forest soil. FEMS Microbiol. Ecol. 63, 181–191.

Fornasier, F., Margon, A., 2007. Bovine serum albumin and Triton X-100 greatly increase phosphomonoesterases and arylsulphatase extraction yield from soil. Soil Biol. Biochem. 39, 2682–2684.

Fornasier, F., Ascher, J., Ceccherini, M.T., Tomat, E., Pietramellara, G., 2014. A simplified rapid, low-cost and versatile DNA-based assessment of soil microbial biomass. Ecol. Indic. 45, 75–82.

Francis, C.A., Roberts, K.J., Beman, J.M., Santoro, A.E., Oakley, B.B., 2005. Ubiquity and diversity of ammonia - oxidizing archaea in water columns and sediments of the ocean. Proc. Natl. Acad. Sci. U. S. A. 102, 14683–14688.

Franke-Whittle, I.H., Goberna, M., Insam, H., 2009. Design, testing and application of real-time PCR primers for the detection of *Methanoculleus*, *Methanosarcina*, *Methanothermobacter* and uncultured methanogens. Can. J. Microbiol. 55, 611–616.

Fravolini, G., Egli, M., Derungs, C., Cherubini, P., Ascher-Jenull, J., Gómez Brandón, M., Bardelli, T., Tognetti, R., Lombardi, F., Marchetti, M., 2016. Soil attributes and microclimate are important drivers of initial deadwood decay in sub-alpine Norway spruce forests. Sci. Tot. Environ. 569–570, 1064–1076.

Goberna, M., Gadermaier, M., García, C., Wett, B., Insam, H., 2010. Adaptation of methanogenic communities to the cofermentation of cattle excreta and olive mill wastes at 37 °C and 55 °C. Appl. Environ. Microbiol. 76, 6564–6571.

Graham, D.W., Knapp, C.W., Van Vleck, E.S., Bloor, K., Lane, T.B., Graham, C.E., 2007. Experimental demonstration of chaotic instability in biological nitrification. ISME J. 1, 385–393.

Harmon, M.E., Franklin, J.F., Swanson, F.J., Sollins, P., Gregory, S.V., Lattin, J.D., Anderson, N.H., Cline, S.P., Aumen, N.G., Sedell, J.R., Lienkaemper, G.W., Cromack, K., Cummins, K.W., 1986. Ecology of coarse woody debris in temperate ecosystems. Adv. Ecol. Res. 15, 133–302.

Harmon, M.E., Fasth, B., Woodall, C.W., Sexton, J., 2013. Carbon concentration of standing and downed woody detritus: effects of tree taxa, decay class, position, and tissue type. Forest Ecol. Manage. 291, 259–267.

Herrmann, S., Bauhus, J., 2012. Effects of moisture, temperature and decomposition stage on respirational carbon loss from coarse woody debris (CWD) of important European tree species. Scand. J. Forest Res. 28, 346–357.

Hermansson, A., Lindgren, P.-E., 2001. Quantification of ammonia-oxidizing bacteria in arable soil by real-time PCR. Appl. Environ. Microbiol. 67, 972–976.

Hervé, V., Ketter, E., Pierrat, J.-C., Gelhaye, E., Frey-Klett, P., 2016. Impact of Phanerochaete chrysosporium on the functional diversity of bacterial communities associated with decaying wood. PLoS ONE, e0147100.

Hoppe, B., Kahl, T., Karasch, P., Wubet, T., Bauhus, J., Buscot, F., Krüger, D., 2014. Network analysis reveals ecological links between N-fixing bacteria and wood-decaying fungi. PLoS ONE, e88141.

Hoppe, B., Purahong, W., Wubet, T., Kahl, T., Bauhus, J., Arnstadt, T., Hofrichter, M., Buscot, F., Krüger, D., 2015a. Linking molecular deadwood-inhabiting fungal diversity and community dynamics to ecosystem functions and processes in Central European forests. Fungal Divers. 77, 367–379.

Hoppe, B., Krüger, D., Kahl, T., Arnstadt, T., Buscot, F., Bauhus, F., Wubet, T., 2015b. A pyrosequencing insight into sprawling bacterial diversity and community dynamics in decaying deadwood logs of *Fagus sylvatica* and *Picea abies*. Sci. Rep. 5, 9456.

Hunter, M.L., 1990. Wildlife, Forests and Forestry: Principles of Managing Forests for Biological Diversity. Prentice Hall, Englewood Cliffs, NJ, USA, p. 370.

Johnston, S.R., Boddy, L., Weightman, A.J., 2016. Bacteria in decomposing wood and their interactions with wood-decay fungi. FEMS Microbiol. Ecol. 92, 1–12.

Kandeler, E., 1993. Bestimmung von Ammonium. In: Schinner, F., Öhlinger, R., Kandeler, E., Margesin, R. (Eds.), Bodenbiologische Arbeitsmethoden. Springer, Berlin, Heidelberg, pp. 366–368.

Klason, P., 1893. Bidrag till kannedomen om sammansattningen af granens ved samt de kemiska processerna vid framstallning af cellulosa darur. Teknisk tidskrift. Afdelningen för kemi och Metallurgi 23, 17–22.

Kowalchuk, G.A., Stephen, J.R., de Boer, W., Prosser, J.I., Embley, T.M., Woldendorp, J. W., 1997. Analysis of ammonia-oxidizing bacteria of the β subdivision of the class Proteobacteria in coastal sand dunes by denaturing gradient gel electrophoresis and sequencing of PCR-amplified 16S ribosomal DNA fragments. Appl. Environ. Microbiol. 63, 1489–1497.

Lauber, C.L., Hamady, M., Knight, R., Fierer, N., 2009. Pyrosequencing-based assessment of soil pH as a predictor of soil bacterial community structure at the continental scale. Appl. Environ. Microbiol. 75, 5111–5120.

Larsen, M.J., Jurgensen, M.F., Harvey, A.E., 1978. Nitrogen fixation associated with wood decayed by some common fungi in western Montana. Can. J. For. Res. 8, 341–345.

Leavitt, S.W., Danzer, S.R., 1993. Method for batch processing small wood samples to holocellulose for stable-carbon isotope analysis. Anal. Chem. 65, 87–89.

Lombardi, F., Cherubini, P., Tognetti, R., Cocozza, C., Lasserre, B., Marchetti, M., 2013. Investigating biochemical processes to assess deadwood decay of beech and silver fir in Mediterranean mountain forests. Ann. For. Sci. 70, 101–111.

Mayo, S.C., Chen, F., Evans, R., 2010. Micron-scale 3D imaging of wood and plant microstructure using high-resolution X-ray phase-contrast microtomography. J. Struct. Biol. 171, 182–188.

Merrill, W., Cowling, E.B., 1966. Role of nitrogen in wood deterioration. IV. Relationship of natural variation in nitrogen content of wood to its susceptibility to decay. Phytopathology 56, 1324–1325.
Mukhin, V.A., Voronin, P.Yu., 2007. Methane emission during wood fungal decomposition. Dokl. Biol. Sci. 413, 159–160.
Mukhin, V.A., Voronin, P.Yu., 2009. Methanogenic activity of woody debris. Russ. J. Ecol. 40, 149–153.
Øvreås, L., Forney, L., Daae, F.L., Torsvik, V., 1997. Distribution of bacterioplankton in meromictic lake Sælenvannet, as determined by denaturing gradient gel electrophoresis of PCR-amplified gene fragments coding for 16S rRNA. Appl. Environ. Microbiol. 63, 3367–3373.
Pan, Y., Birdsey, R.A., Fang, J., Houghton, R., Kauppi, P.E., Kurz, W.A., Phillips, O.L., Shvidenko, A., Lewis, S.L., Canadell, J.G., Ciais, P., Jackson, R.B., Pacala, S.W., McGuire, A.D., Piao, S., Rautiainen, A., Sitch, S., Hayes, D., 2011. A large and persistent carbon sink in the world's forests. Science 333, 988–993.
Petrillo, M., Cherubini, P., Sartori, G., Abiven, S., Ascher, J., Bertoldi, D., Camin, F., Barbero, A., Larcher, R., Egli, M., 2015. Decomposition of Norway spruce and European larch coarse woody debris (CWD) in relation to different elevation and exposure in an Alpine setting. iForest 9, 154–164.
Petrillo, M., Cherubini, P., Fravolini, G., Marchetti, M., Ascher-Jenull, J., Schärer, M., Synal, H.A., Bertoldi, D., Camin, F., Larcher, R., Egli, M., 2016. Time since death and decay rate constants of Norway spruce and European larch deadwood in subalpine forests determined using dendrochronology and radiocarbon dating. Biogeosciences 13, 1537–1552.
Prévost-Bouré, N.C., Christen, R., Dequiedt, S., Mougel, C., Lelièvre, M., Jolivet, C., Shahbazkia, H.R., Guillou, L., Arrouays, D., Ranjard, L., 2011. Validation and application of a PCR primer set to quantify fungal communities in the soil environment by real-time PCR. PLoS ONE 6, e24166.
Purahong, W., Arnstadt, T., Kahl, T., Bauhus, J., Kellner, H., Hofrichter, M., Krüger, D., Buscot, F., Hoppe, B., 2016. Are correlations between deadwood fungal community structure, wood physico-chemical properties and lignin-modifying enzymes stable across different geographical regions? Fungal Ecol. 22, 98–105.
Rajala, T., Peltoniemi, M., Pennanen, T., Mäkipää, R., 2012. Fungal community dynamics in relation to susbstrate quality of decaying Norway spruce (*Picea abies* [L.] Karst.) logs in boreal forests. FEMS Microbiol. Ecol. 81, 494–505.
Rosch, C., Mergel, A., Bothe, H., 2002. Biodiversity of denitrifying and dinitrogen-fixing bacteria in an acid forest soil. Appl. Environ. Microbiol. 68, 3818–3829.
Rotthauwe, J.H., Witzel, K.P., Liesack, W., 1997. The ammonia monooxygenase structural gene amoA as a functional marker: molecular fine-scale analysis of natural ammonia-oxidizing populations. Appl. Environ. Microbiol. 63, 4704–4712.
Sedighi Gilani, M., Boone, M.N., Mader, K., Schwarze, F.W.M.R., 2014. Synchrotron X-ray micro-tomography imaging and analysis of wood degraded by *Physisporinus vitreus* and *Xylaria longipes*. J. Struct. Biol. 187, 149–157.
Shigematsu, T., Tang, Y., Kawaguchi, H., Ninomiya, K., Kijima, J., Kobayashi, T., Morimura, S., Kida, K., 2003. Effect of dilution rate on structure of a mesophilic acetate-degrading methanogenic community during continuous cultivation. J. Biosci. Bioeng. 96, 547–558.
Thybring, E.E., 2013. The decay resistance of modified wood influenced by moisture exclusion and swelling reduction. Int. Biodeterior. Biodegradation 82, 87–95.
Töwe, S., Albert, A., Kleineidam, K., Brankatschk, R., Dümig, A., Welzl, G., Munch, J.C., Zeyer, J., Schloter, M., 2010. Abundance of microbes involved in nitrogen transformation in the rhizosphere of *Leucanthemopsis alpina* (L.) heywood grown in soils from different sites of the Damma glacier forefield. Microb. Ecol. 60, 762–770.
Vainio, E.J., Hantula, J., 2000. Direct analysis of wood-inhabiting fungi using denaturing gradient gel electrophoresis of amplified ribosomal DNA. Mycol. Res. 104, 927–936.
van der Wal, A., Ottosson, E., de Boer, W., 2015. Neglected role of fungal community composition in explaining variation in wood decay rates. Ecology 96, 124–133.
Valášková, V., de Boer, W., Gunnewiek, P.J.K., Pospíšek, M., Baldrian, P., 2009. Phylogenetic composition and properties of bacteria coexisting with the fungus *Hypholoma fasciculare* in decaying wood. ISME J. 3, 1218–1221.
Vestin, J.L.K., Söderberg, U., Bylund, D., Nambu, K., Hees, P.A.W., Haslinger, E., Ottner, F., Lundström, U.S., 2013. The influence of alkaline and non-alkaline parent material on Norway spruce tree chemical composition and growth rate. Plant Soil 370, 103–113.
Wessén, E., Hallin, S., 2011. Abundance of archaeal and bacterial ammonia oxidizers—Possible bioindicator for soil monitoring. Ecol. Indic. 11, 1696–1698.
Zuo, J., Cornelissen, J.H.C., Hefting, M.M., Sass-Klaassen, U., van Logtestijn, R.S.P., van Hal, J., Goudzwaard, L., Liu, J.C., Berg, M.P., 2016. The (w)hole story: facilitation of dead wood fauna by bark beetles? Soil Biol. Biochem. 95, 70–77.